DEFENCE
SCIENCE & TECHNOLOGY

DSTO

L-band VV Clutter Analysis for Natural Land in Northern Territory Areas

Yunhan Dong

DSTO-RR-0254

DEFENCE
SCIENCE & TECHNOLOGY

L-band VV Clutter Analysis for Natural Land in Northern Territory Areas

Yunhan Dong

Electronic Warfare and Radar Division
Systems Sciences Laboratory

DSTO-RR-0254

ABSTRACT

Land clutter is statistical by nature, and its values vary in many different dimensions. This report analyses land clutter characteristics using AirSAR data for airborne L band VV polarised radars. In particular, the report concentrates on the distribution of clutter values with respect to grazing angles for various vegetation communities typically seen in the Northern Territory region in Australia. Future reports will address wider aspects, including spatial distributions and Doppler spectra of clutter sufficient to enable the generation of radar clutter models.

RELEASE LIMITATION

Approved for public release

Published by

DSTO Systems Sciences Laboratory
PO Box 1500
Edinburgh South Australia 5111 Australia

Telephone: (08) 8259 5555
Fax: (08) 8259 6567

AR-012-773
May 2003

APPROVED FOR PUBLIC RELEASE

L-band VV Clutter Analysis for Natural Land in Northern Territory Areas

Executive Summary

This report presents the result of a land clutter study carried out under the task AIR02/232 (AEW&C SUPPORT).

A knowledge of clutter is essential in the estimation of the detection performance of an airborne early warning and control (AEW&C) radar. There is concern that clutter from the Australian environment differs markedly from that of Northern America. Hence estimation of the performance of a system by the radar manufacturer, by whom most clutter data might be collected from Northern America, may not be as accurate as desired. Consequently, we have embarked on this study to deduce the nature of scattering in the Australian environment, especially the Northern Territory region, using synthetic aperture radar (SAR) data collected in the JPL Airborne synthetic aperture radar (AirSAR) campaigns in 1990s. The particular objective of this report is to investigate variation in clutter returns from terrain associated with different vegetation communities in the Northern Territory. Such a study is an essential step towards the development of clutter prediction models so that after clutter cancellation, the detection of small target signals by the radar can be enhanced.

It has now become clear that there is no generally accepted clutter model without land information. It is believed on the historical evidence that a successful approach would have to be strongly empirical and site-specific.

This report emphasizes land clutter analysis. Unlike sea clutter, the variation of land clutter depends on dominant backscattering mechanisms largely determined by geophysical parameters of the land as well as radar parameters. Only if the ground surface has little vegetation, and the surface scattering from the ground dominates, is the clutter pattern analogous to the sea clutter pattern.

Four AirSAR L band VV polarisation scenes with a total area of 60 km^2 containing typical vegetation communities in the Top End region of Australia have been used for the analysis. Because the clutter is species dependent, each pixel required a vegetation label before performing any analysis. A SAR image segmentation technique was applied to separate an image into polygons. With the reference of the ground truth information (vegetation map and land information), each polygon was then labelled with a vegetation class to generate an associated classified vegetation map. After such processing, each pixel in the SAR image had a value of backscattering coefficient, a label of vegetation class and a value of grazing angle. The remaining task of finding the backscattering coefficient distribution for each vegetation class against the grazing angle was straightforward.

The analysis has resulted in the following findings:

- Clutter from the open sea monotonically increased with an increase in the grazing angle. In the Darwin scene, the sea clutter was as low as -22dB at the grazing angle of 20°, whereas the clutter increased to as high as 16dB at the grazing angle of 75°. The actual values of clutter depend on the wind velocity.

- Clutter from all vegetation classes exhibited little dependence on the grazing angle in the region of 20-65°. The clutter of a specific vegetation class statistically remained approximately constant in this region. It is worth noting that 20° is not the lowest angle of the plateau region, rather it is the lowest angle where AirSAR data are available. The lowest angle of the plateau region is believed to be about 5 to 10° at L band.

- Clutter was correlated to vegetation biomass, with a high value of about −10dB for eucalyptus and melaleuca open forests and a low value of about −20dB for bare soil. The dynamic range due to the vegetation was about 8-10dB.

- Quiet river water had the lowest clutter at grazing angles of 30° to 65°. The clutter ranged from -35 to -25dB, some 10-15dB below the clutter of bare soil.

- When the grazing angle increased beyond 70°, all vegetation classes in the Top End, i.e., the region of the Darwin and gulf district in the Northern Territory demonstrated a rapid increase in clutter signals similar to the pattern of the sea clutter. Because all forests in these scenes had less than 30% canopy closure, surface scattering could still contribute to the clutter. The value of the clutter, compared to the value of the sea clutter, would be expected to be lower, due to attenuation by the canopy layer and understorey vegetation as well as the lower dielectric constant of the ground surface. The clutter of calm river water at a grazing angle of near 90°, however, would be many dB higher than that of open seawater.

- These four scenes have not demonstrated a significant difference in the clutter from forests between dry and wet seasons. But we have definitely seen that the return from melaleuca with underwater was a few dB (4-5dB) higher than the return from melaleuca without underwater.

Author

Yunhan Dong
Electronic Warfare and Radar Division

Dr Yunhan Dong received his Bachelor and Master degees in 1980s in China and his PhD in 1995 at UNSW, Australia, all in electrical engineering. He then worked at UNSW from 1995 to 2000, and Optus Telecommunications Inc from 2000 to 2002. He joined DSTO as a Senior Research Scientist in September 2002. His research interests are primarily in radar signal and image processing, and radar backscatter modelling. Dr Dong was a recipient of both the Postdoctal Research Fellowships and Research Fellowships, from the Australian Research Council.

Contents

1. Introduction

Clutter studies are essential for the development of airborne early warning and control (AEW&C) radars. Clutter in an AEW&C radar is unwanted signals from the ground, sea, rain, fog or other precipitation, as well as birds, insects, etc. The amplitude of clutter from land varies over an extremely wide dynamic range depending on radar parameters, grazing angle and the complex variety of surface features and discrete reflecting objects comprising or associated with the terrain. The resultant clutter signal varies in a complex manner with time and space to interfere with and mask much weaker target signals in the radar receiver. Doppler signal processing techniques allow radars to detect targets within clutter regions by exploiting the difference in frequency of the signal returned due target motion compared to that from the relatively stationary clutter. However, the clutter signal is often overwhelmingly stronger than the target signal, and modern pulse radars can remain severely limited by clutter residues when trying to detect small targets. Land clutter studies lead to the establishment of land clutter models and findings of better radar waveforms, so that after clutter cancellation, the detection of small target signals can be enhanced.

Land clutter is better described as deterministic but showing a high degree of complexity such that is can usually be represented as a set of statistical distributions, with each distribution corresponding to the dominant scattering source(s) encountered in a particular localised spatial region. Variation of clutter in space in the down-range dimension is of main concern for the proper adjustment of a target detection threshold value. Large isolated spiky clutter can cause either a false alarm because of a threshold being set too low for the general clutter average, or failure to detect targets because of a threshold being set too high.

The observed variation in Doppler shift from clutter sources is also of importance to a radar system, since Doppler based processing is often employed as a major discriminator against clutter returns. Frequency filtering is often used to remove the clutter. In consequence, the signal of low velocity targets that have Doppler frequency components of the same order as those caused by the motion of clutter may also be filtered away.

The characteristics of land clutter are quite different to those of sea clutter in the majority of cases. The very different surface texture and highly variable dielectric constant of land together with scattering and absorption by vegetation results in substantial variation in land clutter. The reflectivity of ground is strongly dependent upon the surface roughness and the water content of the top few centimetres of the ground surface. Similarly the reflectivity and absorption characteristics of vegetation also depend upon the above ground biomass, the water content as well as the shape, structure and orientation of the plant material. Vegetation and ground surface together consist of even more complex scattering mechanisms.

Land clutter shows significant seasonal variability in many parts of the world. The changes in surface moisture in the environment introduce significant changes in the surface scattering and scattering from plant material. Seasonal variability is also derived from agricultural activity and the presence of deciduous species.

Surface clutter is normally described by the RCS per unit area of the clutter surface, which is normally referred to as the backscattering coefficient (σ_0), or clutter coefficient, or the reflectivity or simply clutter[1] (these names will be used interchangeably in this report), and hence is a dimensionless quantity[2]. For a given transmitter frequency, the power of the return received from a small patch of ground is,

$$P_r \propto \frac{P_{avg} G^2 \lambda^2 \sigma_0 F^4 A_g}{R^4} \tag{1}$$

where P_{avg} - average transmitted power, G - gain of radar antenna in the direction, λ - wavelength, A_g - resolvable area of the ground, R - range of the ground patch and F^4 - the pattern propagation factor.

The definition of backscattering coefficient implies that its mean value is independent of the particular cell size or resolution utilised in a given clutter spatial field. However, the individual spatial samples of $\sigma_0 F^4$ as opposed to their mean, usually depend strongly on the resolution size (Billingsley, 2002). In a situation where dimensions of discrete scatterers, such as buildings, compared to the radar resolution, are not very small, reducing cell size results in more cell-to-cell variability, and increasing spread in values of $\sigma_0 F^4$. Thus the shapes of the broad amplitude distribution of $\sigma_0 F^4$ are highly dependent on resolution.

This report mainly focuses on analysis of L band VV polarisation clutter returns from natural land covered with various types of vegetation, typically seen in the Northern Territory in Australia. The data were collected by the JPL Airborne synthetic aperture radar (AirSAR) System.

In general the backscattering coefficient of natural land is a function of the following parameters:

---

[1] Rigorously speaking, clutter is expressed as $\sigma_0 F^4$, where F is the propagation factor. In attempting to measure clutter levels it is very difficult in most cases to measure the value of F over large areas. Estimating the value of F is fraught with practical problems, so that for practical purposes clutter is characterised by the moments of $\sigma_0 F^4$ and not by σ_0.

[2] Whilst dimensionless, σ_0 is popularly expressed as m^2/m^2 in the linear scale and dBm^2/m^2 in the dB scale, or simply dB in the dB scale. This report expresses it as dB in the dB scale.

- Wavelength;
- Polarisation;
- Local grazing angle;
- Local aspect angle;
- Vegetation (species, structure, density, biomass etc);
- Surface conditions (roughness and moisture content).

At low grazing angles, clutter measurements over terrain have found that the resulting clutter spatial amplitude distributions are highly skewed. The measured broad distributions are of highly variable shapes with mean-to-median ratio as high as 15 or even 30dB (Billingsley, 2002). Because the reflectivity is not merely a function of radar parameters (frequency, polarisation, resolution and depression angle), any land clutter model that attempted to represent the clutter without accommodating the variability in land topography, and land vegetation cover (and the moisture levels of the environment) would at best generate a poor approximation. It has now become clear that there is no generally accepted clutter model without land information. It is believed on the historical evidence that a successful approach would have to be strongly empirical and site specific (Billingsley, 2002). Land clutter modelling would probably be endless as time passes because of the great variety of terrain and the inability to describe it precisely.

To analyse land clutter data, therefore, we need not only the radar parameters, but also the information (with a high degree of fidelity) of terrain elevation, the ground truth and the possibly the moisture levels of the environment when the clutter data is collected. While the digital terrain elevation data (DTED) and geographical information system (GIS) may provide the land terrain elevation and land usage, respectively, the moisture level of the environment may rely on meteorological data.

This report contains an analysis of the land clutter data obtained from SAR images generated by the NASA/JPL L band AirSAR data collections carried out in the Northern Territory. Future reports will address wider aspects including the fitting of statistical distributions, and the observed clutter Doppler spectrum sufficient to enable the generation of radar clutter models.

2. Land Clutter Concepts

2.1 Basic Backscatter Mechanisms

The interaction between electromagnetic waves and the natural environment is complex. Analytical solutions exist for a number of simple scattering shapes, but in general are only of use when assumptions in the analytical model closely match the situation. Often such a situation only exists in the laboratory conditions. By far only a few scatterers that have simple geometries, such as dielectric needles (modelled for needle-like leaves and twigs), disks (for broad leaves) and cylinders (for trunks and branches) have analytic solutions. If we have a close look at trees around us, these

assumptions are still too ideal to model the real world. For example, the analytic solution to a bunch of dielectric needles, in which the distances among needles are so close that the near field interactions among needles cannot be ignored, is still not available. Nevertheless, theoretical modelling helps understanding of scattering mechanisms better, explain various phenomena observed and to provide guidelines for designs of the optimal radar parameter and waveforms to differentiate target signals from clutter signals.

Based on the understanding of the relative importance of the different scattering mechanisms, a phenomenological model for backscattering from a forested area can be constructed by summing up contributions of different forest components considered to be more significant than the rest. The addition is normally in the power domain as scatterers are randomly distributed in space. As shown in Figure 1 the dominant backscattering mechanisms for a forested area are (Ranson and Sun, 1994, Dong, 1995):

1. Surface backscattering;
2. Trunk-ground double bounce scattering;
3. Branch/trunk direct backscattering;
4. Multiple crown-ground scattering;
5. Crown volume scattering.

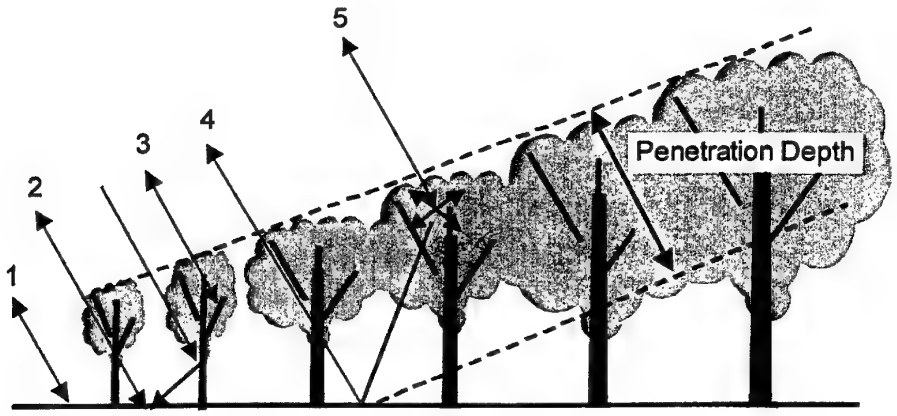

Figure 1: Dominant radar backscattering mechanisms for a forested area

The two-way attenuation caused by the canopy layer has to be considered if the mechanism happens beneath the canopy.

Relative contributions of the above mechanisms vary depending on vegetation conditions and radar parameters. If the wavelength is short (X or C band), the penetration depth of electromagnetic waves is very limited. The total contribution thus mainly consists of scattering from the top layer of the canopy and the canopy-free ground surface, but little from trunk-ground and crown-ground double bounce scattering mechanisms, since the incoming microwaves have been attenuated by the

foliage layer before reaching the lower layers. Besides, to short wavelength radars, the ground surface is rougher, which further weakens the contribution from double bounce scattering mechanisms. On the other hand, if the wavelength is long (L band, for example), the penetration depth can reach a few metres even for a moderately dense canopy (the above ground biomass up to about 100 tons per hectare), so mechanisms beneath the canopy layer can still make contributions. Trees in most open woodland in the Northern Territory region are generally sparsely distributed with about 30% foliage closure, and the biomass is generally less than 100 tons/ha. Tiangco (1999) combined from literatures including Imhoff (1993), Dobson et al (1992, 1995a, 1995b), Karam et al, (1995), Harrel et al (1995), Hsu et al (1993) Christensen et al (1990), and Souyris and Le Toan (1995), the L band HH backscattering coefficient as a function of pine/conifer biomass as shown in Figure 2. It can be seen that most observations start to saturate when biomass approach 100 tons/ha. The dynamic range of the L band HH backscattering coefficient due to the presence of forests for a fixed grazing angle in the plateau region[3] is about 7 to 10dB. In other words, the variation of land clutter for a fixed grazing angle in the plateau region is from 7 to 10dB depending on how much biomass is above the ground. In addition, for the same biomass, the backscattering coefficient at the L band HH polarisation can also vary about 4dB, depending on the species, tree structures, ground surface roughness, soil moisture etc. It is understood that in general the VV backscattering coefficient should have a similar pattern but a few dB below the HH data as shown in Figure 3 (Dobson, et al, 1992).

If the ground is wet (so the dielectric constant is high) and the surface is smooth, the double bounce scattering from the trunk-ground and crown-ground mechanisms may become dominant. In this situation, vertical trunks contribute the most. It has been found that the backscattering coefficient of a forested area can be more than 8-10dB higher when it is flooded compared to un-flooded conditions (Richards at al, 1987). If data are collected at a single polarisation, there is no way to tell whether the contribution is due to odd-bounce (single bounce and triple-bounce) or even-bounce (double-bounce) scattering mechanisms. However if multipolarised data is collected, statistically, contributions of odd-bounce and even-bounce scattering mechanisms can be determined, because the angle differences between HH and VV are 0° and about 180°, respectively for odd-bounce and even-bounce scattering mechanisms (Dong et al, 1998).

---

[3] Plateau region is the region of grazing angle where the variation of $\sigma_0 F^4$ is slow. The other two regions where the variation of $\sigma_0 F^4$ is fast, are near grazing incidence region and near vertical incidence region, respectively. The dominant scattering mechanisms in these three regions are usually different. However, the boundaries of the three regions change with wavelength, polarisation and landcover (Long, 2001). See Figure 7 for a general separation of the three regions.

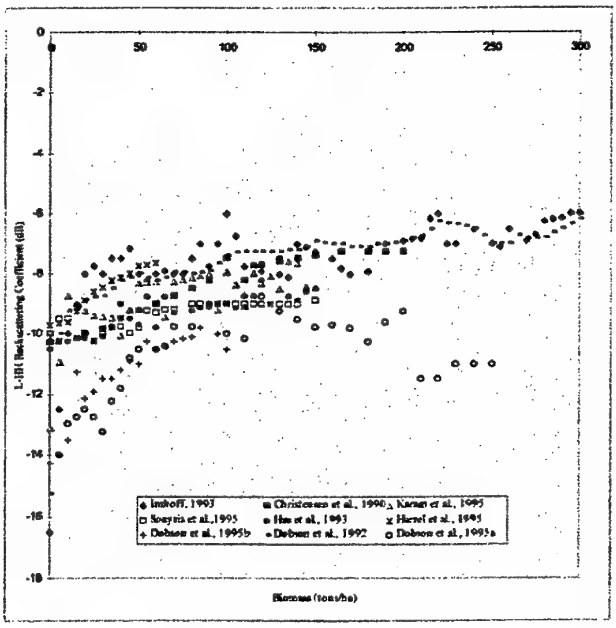

Figure 2: L band HH backscattering coefficient as a function of pine/conifer biomas (tons/ha) for the grazing angle in the plateau region of 30-60 degrees (combined by Tiangco, 1999)

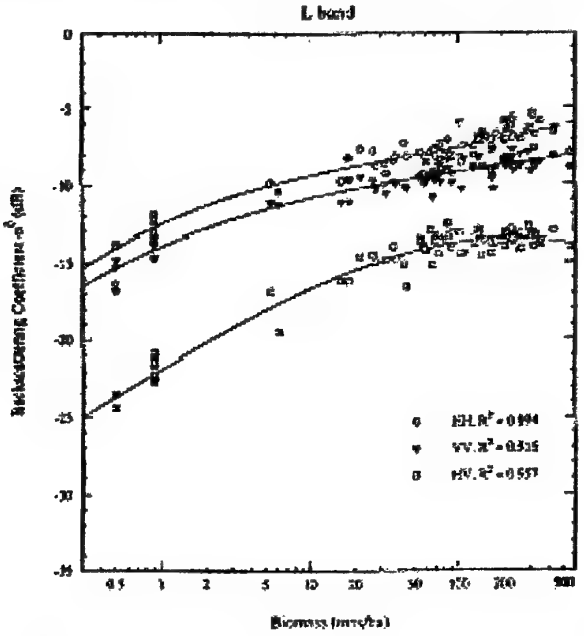

Figure 3: L-band backscatter as a function of the log of total aboveground biomass (tons/ha) of maritime pine and loblolly pine (Dodson, et al, 1992)

2.2 Seasonal Dynamics

The climate in the Top End, i.e., the region of the Darwin and Gulf district in the Northern Territory, is monsoonal, with distinct wet (November to April) and dry (May to October) seasons. The appearance of vegetation communities in these two seasons is also distinctly different. Figure 4 (a) shows the growth in understorey vegetation in January, the height of the wet season in Kakadu National Park (13.0°N, 132.5°E). The same scene in October, Figure 4 (b), near the end of the dry season has virtually no herbaceous plant material (AUSLIG, 1990). The corresponding clutter distribution will be different, not only due to the existence of the understorey vegetation and more leafy biomass on trees, but also due to the significant difference in the dielectric constant of the ground surface in the wet season. For very dry soil, the dielectric constant can be as low as $3-i1$, while the dielectric constant of wet and saturated soil can approach the dielectric constant of water, which is about $79-i59$ (seawater[4], L band) or $80-i0$ (fresh water, L band) (Stogryn, 1971). The seasonal variation of the backscattering coefficient for some areas therefore can be as high as more than 8-10dB.

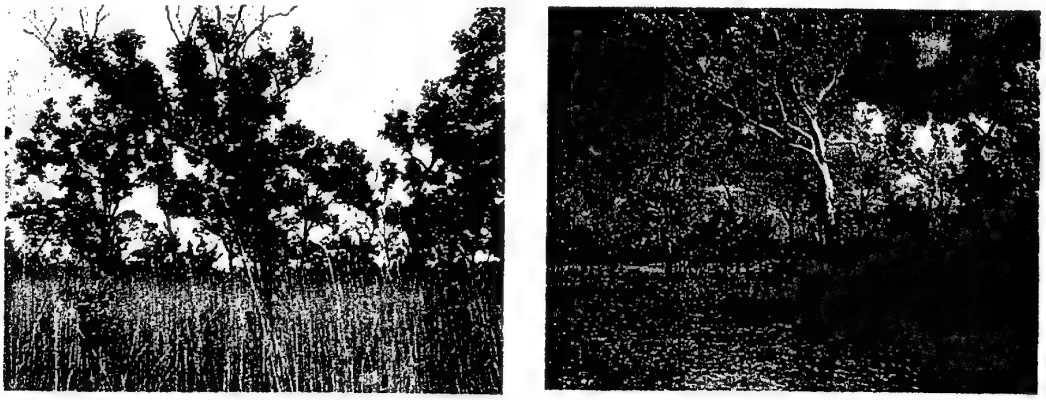

(a) (b)

Figure 4: The appearance and disappearance of understorey vegetation in wet and dry seasons, respectively. Photos were taken in January (Wet) and October (Dry) in Kakadu National Park (AUSLIG, 1990)

For illustration purposes, Figure 5 shows a sequence of RADARSAT (C band, HH polarisation) SAR images of the South Alligator River (12.3°N, 132.4°E), the Northern Territory, acquired in February, May and September, respectively, in 1998 (Horn et al 2001). The September (end of the dry season) image, Figure 5 (c), clearly depicts the South Alligator River and its adjacent floodplain whose grassland cover retained only isolated patches of trees or woodland. The February image (middle of the wet season), Figure 5 (a), shows the widespread nature of the wet conditions. Due to the extensive grass cover of the floodplain initiated by rain, the boundary between the saturated

[4] Value for seawater is variable, depending upon frequency, temperature, salinity and suspended solids.

floodplain and the saturated woodland became difficult to detect as shown in Figure 5 (b). Some bright patches (possibly shrubs or small trees) in the floodplain area shown in the wet season image disappeared in the dry season image indicating that these areas were possibly flooded when the wet image was taken, so that there might be a strong component of double bounce return in the wet image for these areas.

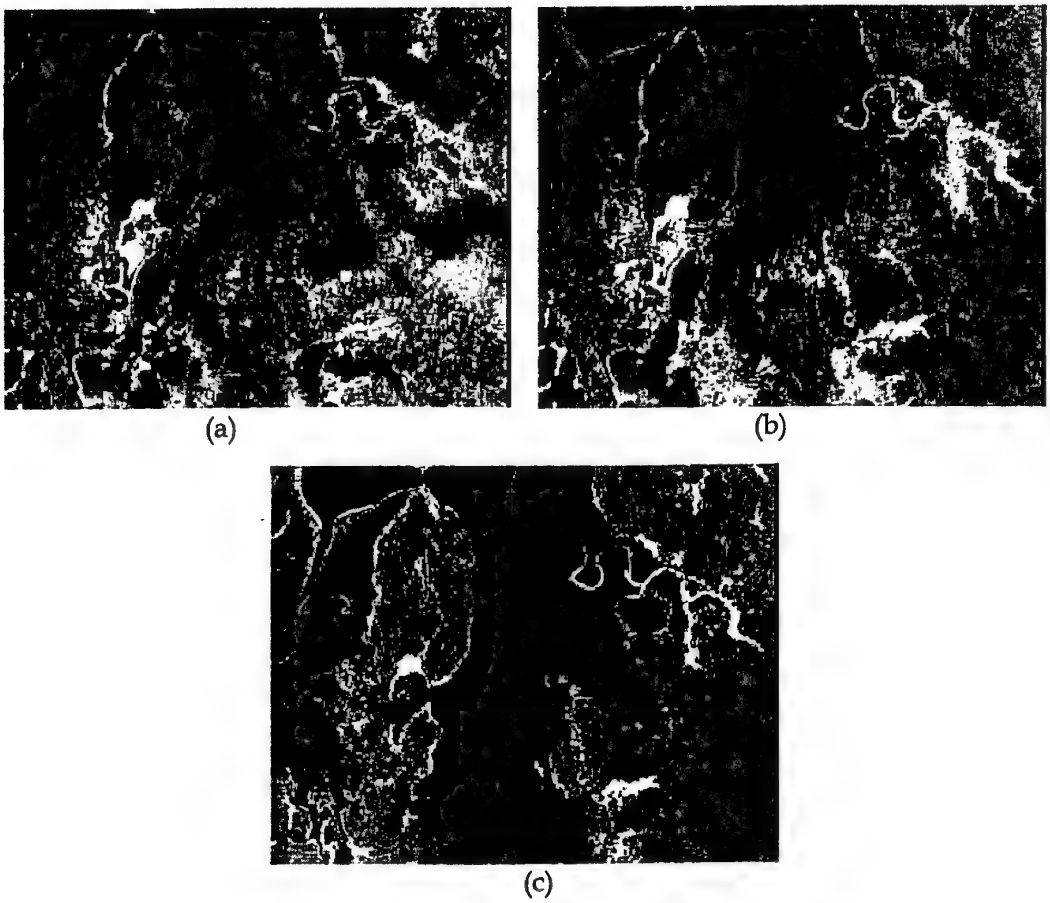

Figure 5: RADARSAT C band HH multitemporal imagery of South Alligator River, the Northern Territory, acquired in (a) February, middle of the wet season, (b) May, end of the wet season and (c) September, end of the dry season, 1998, respectively

2.3 Effects of Surface Topography

Surface topography is well known to have a significant impact on land clutter. Local slopes alter the local grazing angle and the local aspect angle. It would not be possible to extract meaningful clutter data unless the variation in topography were accommodated in the analysis, if the topography were a dominant source of scattering. The greater the variability in the topography is, the greater the variation in local

grazing angle and the local aspect angle. Figure 6 depicts the change in local grazing angles due to topographic slopes. If we draw the picture in 3D, we would also be able to demonstrate the change in the local aspect angle. To compute the backscattering signal, if the scattering mechanism is polarisation dependent, the incident wave, even if it is single-polarised, will have to be decomposed into local V and H components with respect to the local coordinates. Each component might generate co- and cross-polarised backscattered signals with respect to the local coordinates. These four components will again have to be transformed back to the radar's coordinate system in order to work out the final co and cross-polarised components to the radar's receiving antenna. According to geometry, the normal of the local surface is:

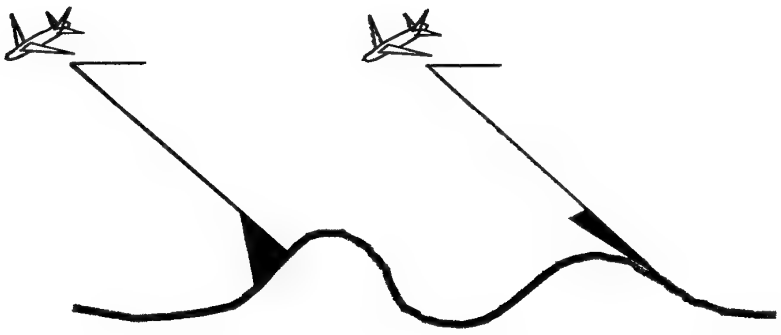

Figure 6: Local grazing angle is altered due to topographic slopes (radar's grazing angle in yellow and local grazing angle in pink)

$$\hat{n} = \frac{-\hat{x}\xi_x - \hat{y}\xi_y + \hat{z}}{\sqrt{1+\xi_x^2 + \xi_y^2}} \tag{2}$$

where ξ_x and ξ_y are the surface slopes in the x and y directions respectively. The local grazing angle becomes,

$$\beta = \frac{\pi}{2} - \cos^{-1}(\hat{n}_s \cdot \hat{n}) \tag{3}$$

where $\hat{n}_s$ is the backscattering direction. The local horizontal and vertical polarisation directions are:

$$\hat{h} = \frac{\hat{n} \times \hat{n}_s}{|\hat{n} \times \hat{n}_s|} \tag{4}$$

$$\hat{v} = \hat{n}_s \times \hat{h} \tag{5}$$

If the local slopes are equal to zero, the normal of the local surface coincides with the z direction, so do the local horizontal and vertical polarisation directions with the radar's polarisation directions.

2.4 Land Clutter Pattern

Sea clutter has a distinct pattern in which the backscattering coefficient monotonically increases with an increase in grazing angle (except when the grazing angle approaches 0° the clutter climbs abruptly (Nathanson, et al, 1999). In general we cannot simply draw an analogy between the land clutter pattern and the sea clutter pattern. If there is little vegetation (bare soil, desert etc), this analogy might be right. But still we have to remember that the dielectric constant of the top surface layer of the ground (top 1-10 cm) is generally much smaller than that of seawater, resulting in lower clutter return, even if the surface roughness is about the same. An increase in vegetation biomass increases returns for the grazing angle in the low and plateau regions. In the high grazing angle region, on the other hand, the existence of vegetation will significantly reduce the clutter return. This is because at a high grazing angle, the return is mainly dominated by specular reflections from facets perpendicular to the radar, but the existence of vegetation forms a layer of attenuation medium that attenuates the signal. Also the Fresnel reflection coefficient (a function of dielectric constant and incidence angle) of the ground surface is substantial smaller than that of the seawater.

An extreme condition of vegetation is that if forests have a dense and closed canopy (eg, tropical rainforests and vine thickets), and its thickness is greater than the radar's penetration depth, then the backscatter is dominated by canopy volume scattering and the variation of the backscattering coefficient with the grazing angle vanishes. If the orientation of leafy components is further uniformly distributed in space, then the backscattering coefficient eventually becomes independent of the grazing angle (analogous to the radar cross-section of a sphere independent of the incidence angle) – a totally different pattern compared to the sea clutter pattern.

In summary, there is no single pattern that can describe land clutter and thus clutter models have to be site specific. Therefore in addition to radar parameters, the land clutter is also dependent on vegetation and topography of the site, and the weather conditions when the radar is used. For illustration purposes, Figure 7 depicts differences among the clutter patterns of bare soil, open woodland and closed forest at L band VV polarisation.

We will demonstrate these differences when we look into details of SAR data in Section 4.

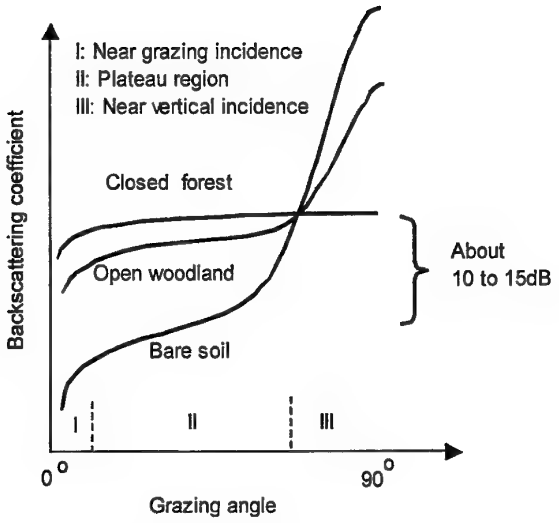

Figure 7: Depiction of L band VV land clutter pattern varying from bare soil to closed forest

3. Analysis Methods

The terrain encountered in the region under analysis shows very little variation in elevation at the granularity of the available digital terrain data (100 m by 100 m resolution). In the absence of evidence to the contrary we have assumed in our analysis that the impact of the small variations in terrain in this data set is sufficiently small to enable the effect to be ignored in the analysis (the grazing angle of most available data is in the plateau region, not very sensitive to land clutter). Clearly however, to more undulating terrain, local grazing angle variations would need to be accommodated.

3.1 AirSAR Data Decoding

The NASA/JPL AirSAR data are provided in the form of a Stokes matrix and we have extracted from the recording the L band data for VV polarisation using the transformation contained in Appendix A. To enable this analysis we have converted the slant range information to ground range and grazing angle using the transformations in Appendix B. Estimation of the pattern propagation factor has not been attempted, and so the backscatter coefficient estimates derived from the analysis are actually those of $\sigma_0 F^4$ and not just σ_0.

3.2 Image Segmentation

We relied on the GIS (Geographical Information System) information and vegetation map, provided by Vegetation Mapping Group, Department of Primary Industries, Water and Environment, Australia, and Natural Resources Division, Department of

Lands, Planning and Environment, Northern Territory, to determine the vegetation class for each pixel in a SAR image. However, when correlating the vegetation map to the SAR image, we found it extremely difficult to correctly co-register them together, not due to systematic errors (coordinates given in the AirSAR data are often not correct) or distortions in the SAR images (which can be rectified using more control points), but mainly due to inaccuracies in the vegetation map and perhaps the natural shifts of vegetation boundaries. Figure 8 shows the SAR image of the Munmarlary site and its corresponding vegetation map. A simple visual inspection would tell us that we would not be able to use the vegetation map to interpret the vegetation types for each pixel in the SAR image, because the positions and shapes of vegetation boundaries given in the vegetation map are so different from the real positions and shapes shown in the image. To solve this problem, a SAR image segmentation technique (Dong et al, 1999 and 2001), was first applied to the SAR image to locate the vegetation boundaries in the image. Figure 9 shows a portion of the image (so the edges can be viewed clearly) superimposed with the boundaries found.

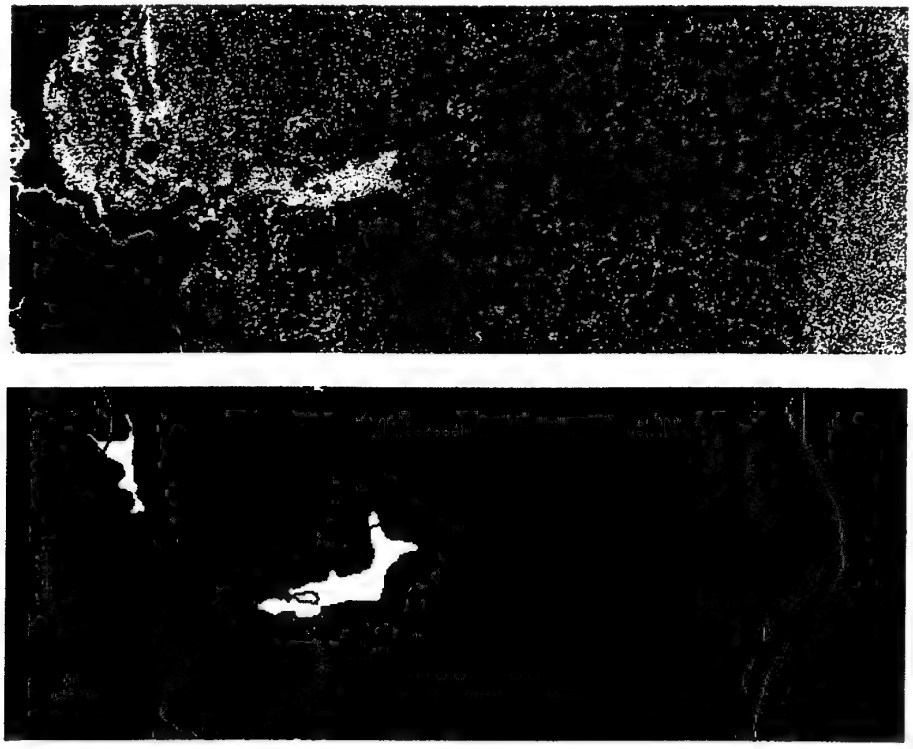

Figure 8: The SAR image and its corresponding vegetation map for the Munmarlary site located in Kakadu National Park. The range direction is from left to right. The ground size of the image is about 8.3 km by 21.3 km

3.3 Image Classification

The classification of the image is based on the segmentation and the vegetation map. After an image is segmented, each segment is visually examined with the reference of the vegetation map and a vegetation label is then attached accordingly. Some classes obviously missed in the vegetation map but shown in SAR images have been added. For instance, mangrove along a creek is shown in the SAR image but not shown in the vegetation map (see Figure 8). The final result of classification is shown in Figure 10. In general, we believe that the vegetation boundaries found in this way are much more accurate than the boundaries given in the vegetation map as shown in Figure 8. Similar procedures have been used to classify other three SAR scenes.

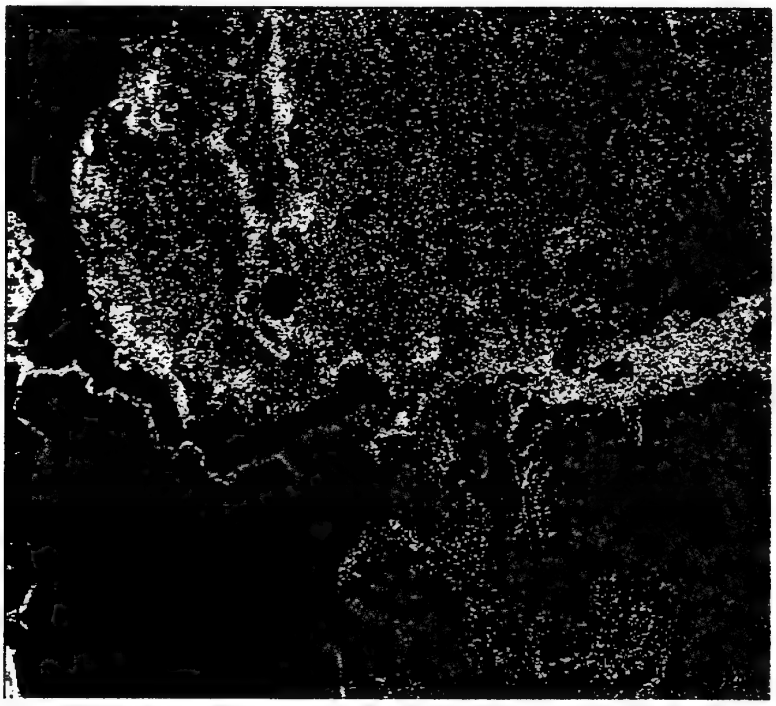

Figure 9: Vegetation edges detected using the SAR image segmentation technique

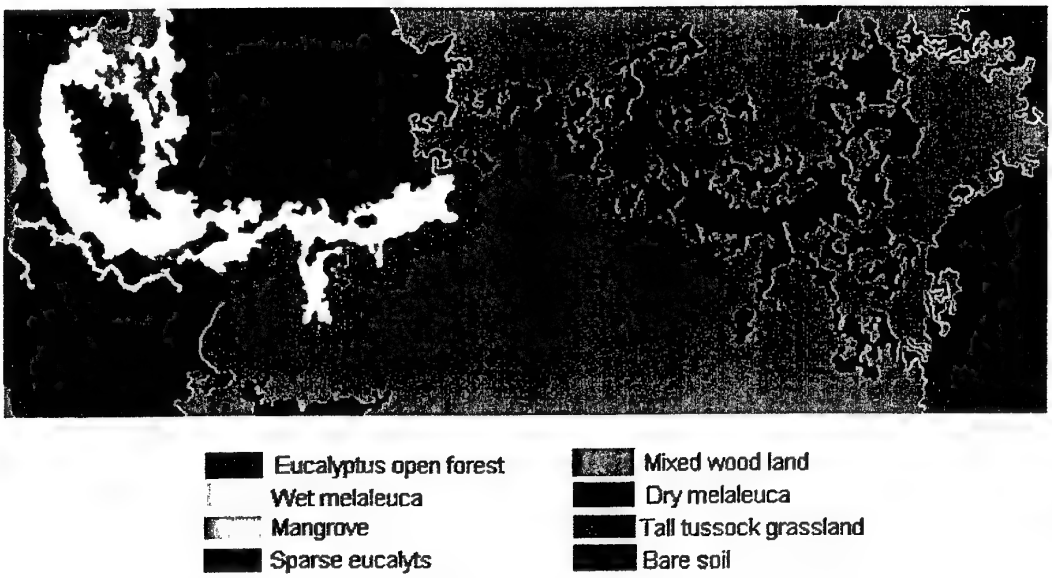

Figure 10: Image classification based on the image segmentation and with the reference of the vegetation map

After classification, each pixel has a value of backscattering coefficient, a label of vegetation class and a value of grazing angle. The remaining task to find the backscattering coefficient distribution for each vegetation class against the grazing angle is straightforward. The next section presents the result.

4. Land Clutter Distributions against Grazing Angles and Vegetation Types

Four L band VV AirSAR sites in the Northern Territory region have been studied in this report. Table 1 lists their locations, acquisition dates and areas.

Table 1: Details of four AirSAR sites

Site	Acquisition date	Location	Area (km^2)
Darwin	15/9/00	12.5°N, 130.8°E	35.7
Munmarlary, Kakadu National Park	24/9/93	12.4°N, 132.4°E	9.6
Humpty Doo	23/11/96	12.7°N, 131.1°E	6.4
Farewell, Kakadu National Park	22/11/96	12.0°N, 132.7°E	11.8

The vegetation in these four sites includes eucalyptus open forests/woodland, mixed woodland, melaleuca open woodland, mangrove, samphire shrub, tussock grassland, bare soil, seawater and river water. If not all, at least the most typical vegetation

communities in the Northern Territory have been included in these four sites. Table 2 shows the major vegetation communities found in the Northern Territory.

Table 2: Present native vegetation in the Northern Territory (ANRA, 2002)

Major vegetation group	Area (1000 km^2)
Hummock grassland	490
Eucalyptus open forest/woodland	354
Acacia shrub / open woodland	165
Tussock grassland	84
Mallee woodland / shrub	35
Chenopod and samphire shrubs	34
Other forests and woodlands	29
Melaleuca forests and woodland	19
Other grasslands, herblands, sedgelands and bushlands	8
Mangroves, tidal mudflats, samphires and bare areas lagoons, lakes	5
Other shrublands	5
Rainforests and vine thickets	1

4.1 Darwin Site

Figure 11 shows the SAR image of the Darwin site and its associated vegetation classification.

Photos of the typical eucalyptus open forest/woodland and samphire shrub are shown in Figure 12 and Figure 13 to provide a general view of these vegetation communities. It has to be pointed out, however, that the photos were not taken at the same location, so appearances of the real vegetation communities on the site may look different.

The backscattering coefficient for each vegetation class as a function of the grazing angle, together with the backscattering coefficient for open sea, are shown in Figure 14. It can be seen that the backscattering coefficient of open sea monotonically increases with an increase in grazing angle. It varies from -18dB at a grazing angle of 20° to 16dB at a grazing angle of 75°. At low and plateau grazing angles, the contribution of sea clutter mainly arise from the Bragg scattering mechanism (Ulaby et al, 1982) resulting in low return signals. As grazing angle increases, more and more local facets will be perpendicular to the backscattering direction and make mirror-like reflections leading to a significant increase in the backscattering coefficient. Therefore, the sea clutter depends on not only the grazing angle, but also sea status determined by the wind velocity. Details of sea clutter modelling and calculation are available elsewhere (Choong, 2000). The wind velocity recorded was 3.89m/s, or 7.6knots, and the sea state may be described as slight or State 2 (Nathanson, 1999) when the SAR data were collected. Compared to the normalised mean sea clutter data given by Nathanson (1999), the sea clutter shown in Figure 14 is about 10dB higher. This might be due to

that fact that the sea surface of littoral is rougher than that of fully developed open seawater.

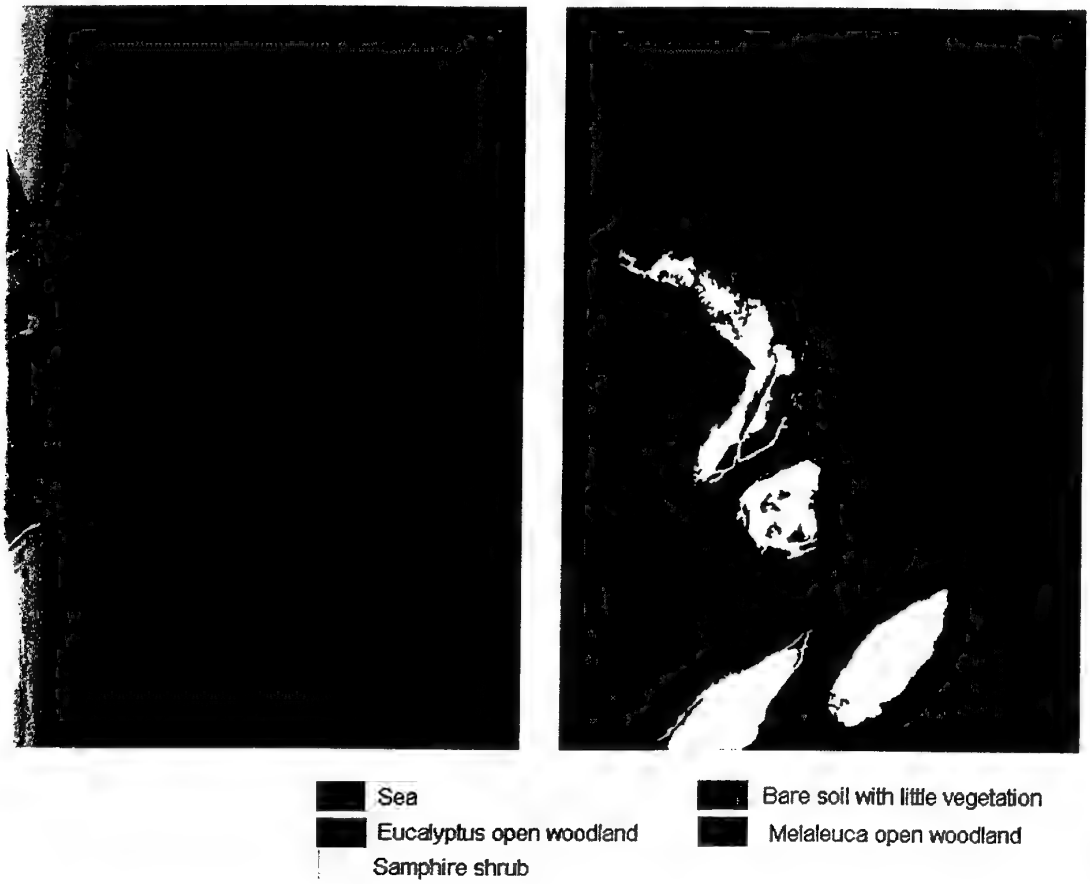

Figure 11: Image of the Darwin site and its accompanying vegetation classification. The range direction is from left to right. The size of the image is about 30.7 km by 21.5 km

Figure 12: Typical eucalyptus open forest/woodland seen in Top End areas: (left) eucalyptus open forest in wet season, 30 km southeast of Darwin (DIPE, 2002) and (right) eucalyptus open forest in the beginning of the dry season, south of Darwin (AUSLIG, 1990)

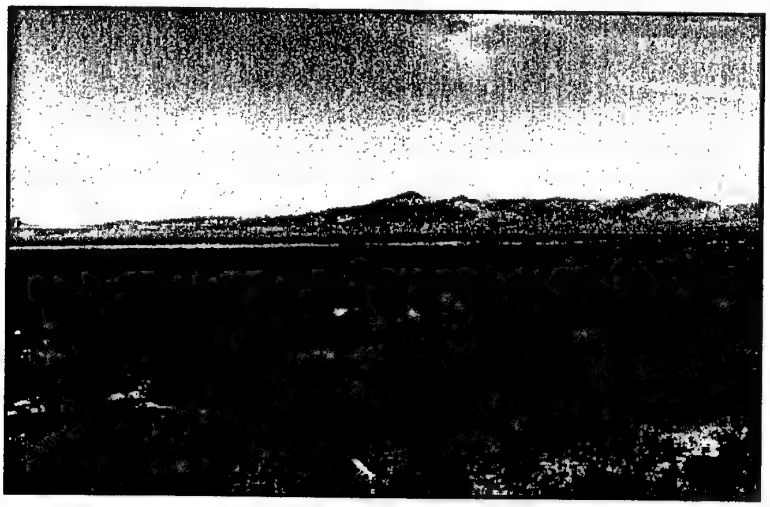

Figure 13: Intertidal samphire shrub seen in Pt Patterson Northern Spencer Gulf, South Australia (http://www.environment.sa.gov.au)

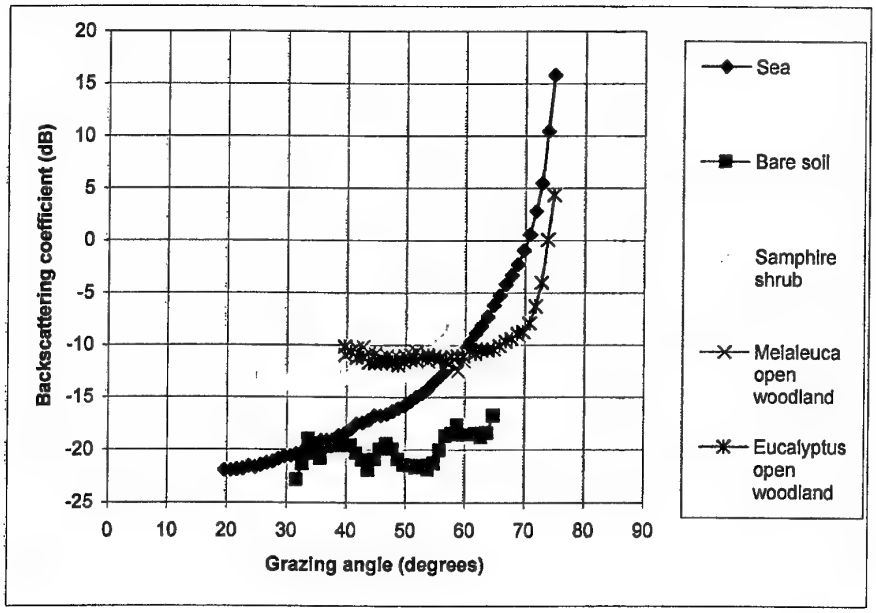

Figure 14: The L band VV clutter distribution for each vegetation class as well as open seawater as a function of grazing angle (Darwin scene)

Clutter from vegetated areas differs from clutter from the sea. For the same vegetation class, the return varies little for grazing angles from 20° to 70°. The dynamic range for different vegetation classes shown in Figure 14 is about 8-10dB, from -20dB for bare soil to about -10dB for eucalyptus/melaleuca open woodlands. Vegetated areas generally have higher clutter returns than the sea for grazing angles less than a certain angle (60° in this particular scene), since scattering mechanisms other than surface scattering are dominant in this region. Bare soil has the lowest clutter because the surface scattering mechanism is the only contributor. Because the image was acquired in September, near the end of the dry season, it is believed that there was not much vegetation above the bare soil. When the grazing angle exceeds 70 degrees, the clutter signal from the eucalyptus open woodland also increases with each increase in grazing angle. From Figure 12 we can see that the canopy of the eucalyptus open woodland covers less than 30% of the ground surface. Therefore, the surface scattering mechanism starts dominating, and the clutter signal follows a pattern similar to that of the sea. The absolute value, though, is still about 10dB below the clutter signal of the sea (for this scene). The interpretation is that the canopy layer attenuates microwave signals, and secondly, the dielectric constant of the ground surface is much lower than that of seawater. We can further deduce that if the ground surface is wetter and smoother, the return will be higher. On the other hand if forests are denser and the canopy is thicker and closed, there will be little increase in clutter signals even at the grazing angle of 90° as the canopy layer attenuates the incident wave so that it hardly penetrates through, and there is little or no signal back from the ground surface.

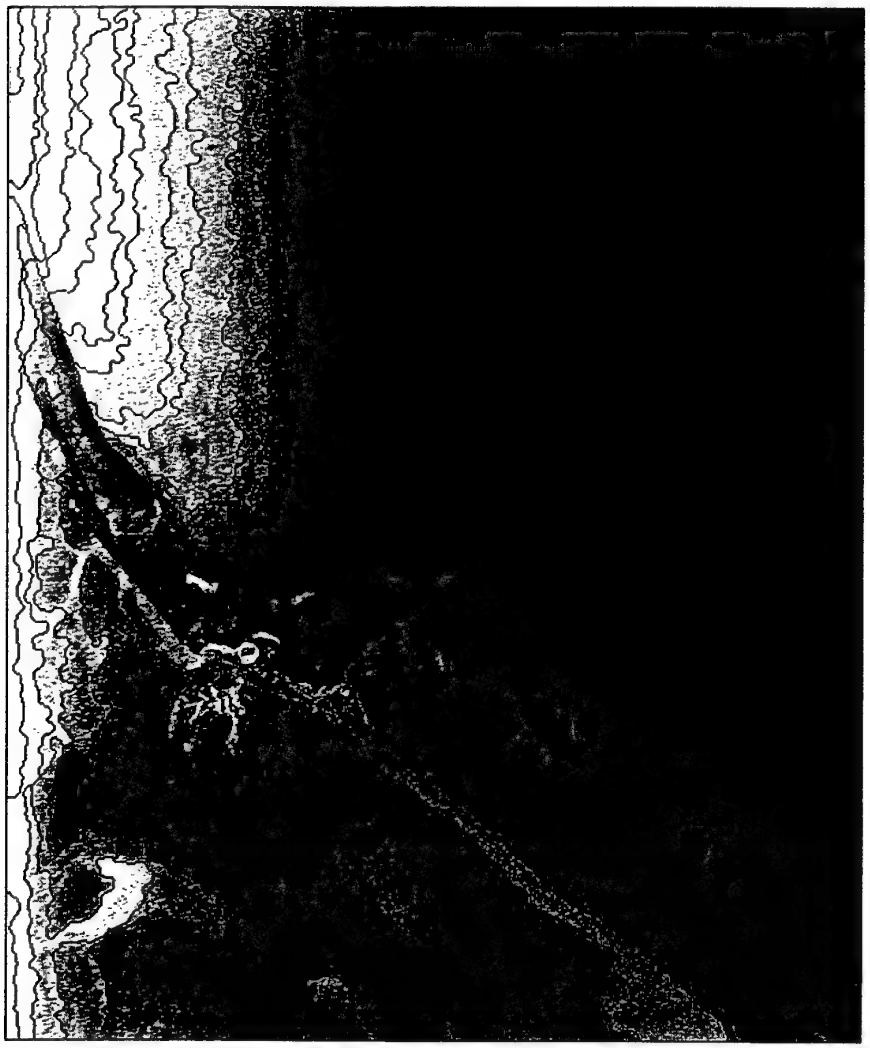

Figure 15: Vertically parallel edges in the sea surface indicate sea clutter to be a function of the grazing angle if all other conditions are the same. In vegetated areas, edges separate different types or densities of vegetation, and the grazing angle plays little role in the low and plateau regions

It is interesting to view the result of segmentation for the Darwin scene. Figure 15 shows a part of the scene with superimposed edges in red. In general, there are no obvious edges in the sea surface area, and values of the clutter decrease gradually with a decrease in grazing angle. However, for the given criteria in segmentation processing (eg, the number of segments in the scene), areas with values statistically different from their surroundings would be separated. Edges in the sea area are all vertically parallel,

indicating that the sea clutter is a function of the grazing angle, if all the other conditions are the same. Also intervals between these vertically parallel edges widen along with a decrease in grazing angle, indicating that the slope of the backscattering coefficient is not constant but decreases with a decrease in grazing angle (However this is only a general description, because we have to notice that the decrease in grazing angle also slows down with increases in ground range). These phenomena disappear in vegetated areas especially in the plateau grazing angle region. In vegetated areas, edges separate different types or densities of vegetation, regardless of the grazing angle, indicating that the grazing angle does not play a critical role any more. This has been demonstrated in the clutter distributions shown in Figure 14 and will also be demonstrated in some of the following figures.

4.2 Munmarlary Site

The SAR image of the Munmarlary site has been shown previously in Figure 8 with its associated vegetation classification in Figure 10. This site is located in Kakadu National Park, covering typical vegetation communities in the Top End. Melaleuca is another common vegetation seen in the region. Figure 16 shows a photo of melaleuca open forest in water swamp areas. Photos of tussock grassland are shown in Figure 17. It can be seen that the appearance of this community can be quite different in dry and wet seasons.

Figure 16: Melaleuca open forest in water swamp areas in Kakadu National Park (ANRA, 2002)

Astrebla pectinata tussock grassland, south west of Mount Isa, QLD.

Astrebla lappacea tussock grassland (dry), south east of Winton, QLD.

Figure 17: Appearances of tussock grassland in dry and wet seasons (ANRA, 2002)

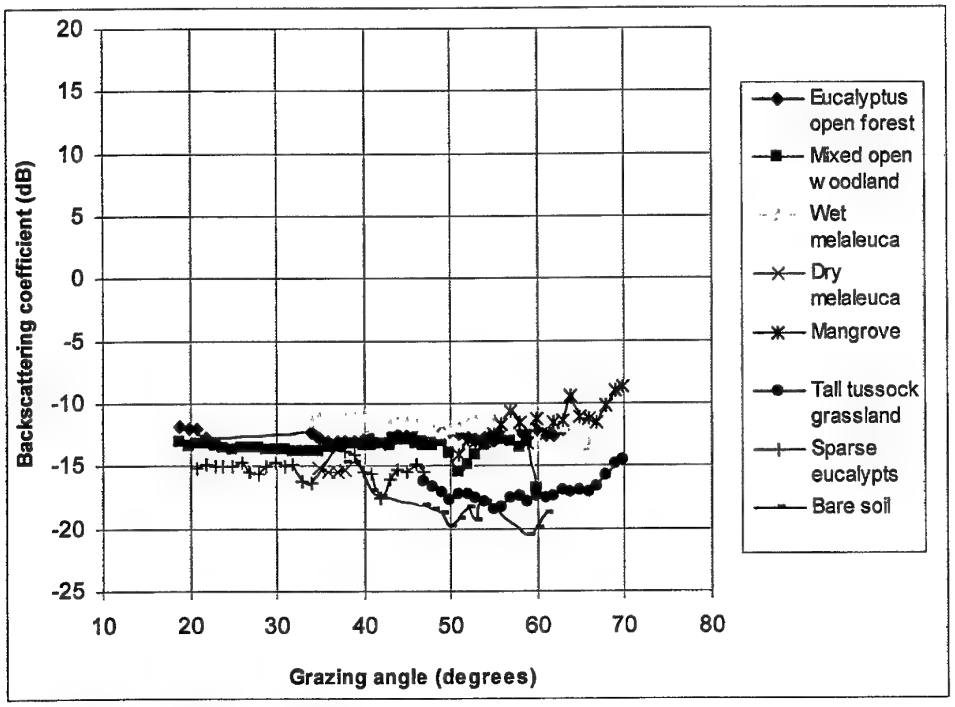

Figure 18: L band VV clutter distribution for each vegetation class as a function of grazing angle (Munmarlary scene)

Figure 18 shows the clutter distribution for each vegetation class against the grazing angle in the Munmarlary scene. In order easy to compare with the clutter distributions shown in Figure 14, we have used the same scale for the vertical axis. It can be seen again that the clutter distributions for all types of vegetation are fairly flat with grazing

angles in the region of 20° to 70°. Clutter values for the wet melaleuca and mangrove are the highest in the scene because of the underwater. Clutter values for the bare soil and tussock grassland are the lowest. In September, the end of the dry season, the grassland would appear as bare soil. The difference of clutter between lowest (bare soil) and highest (wet melaleuca and mangrove) is about 8dB. We can also see there is a tendency of clutter to increase when the grazing angle exceeds 70° due to the increase in surface backscattering contributions as explained previously. Unfortunately, the AirSAR system was in generally unable to sense images with grazing angles greater than 70°.

4.3 Humpty Doo Site

Humpty Doo is a small town about 35km east of Darwin. Figure 19 shows the image of the scene and its accompanying vegetation classification. It has been noted that at the right of the scene there is a residential area, in which some spiky dots are due to the built targets including houses and cars. It is believed that the houses are relatively sparse, so that statistically the clutter is still dominated by the vegetation (the spatial distribution would be broader, though). Therefore we have not separated this area from the surrounding vegetation.

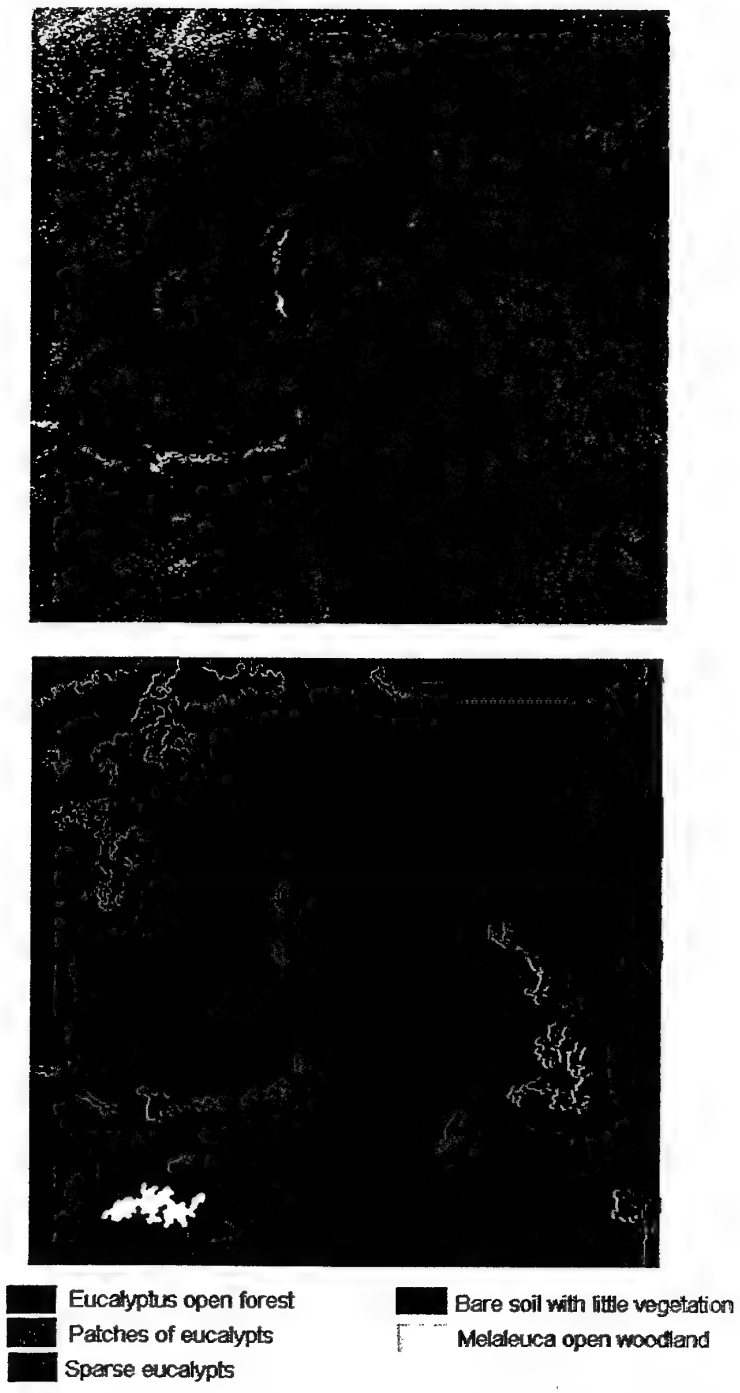

Figure 19: L band VV AirSAR image of the Humpty Doo site and its accompanying vegetation classification. The range direction is from left to right. The image size is 7.5 km by 7.9 km

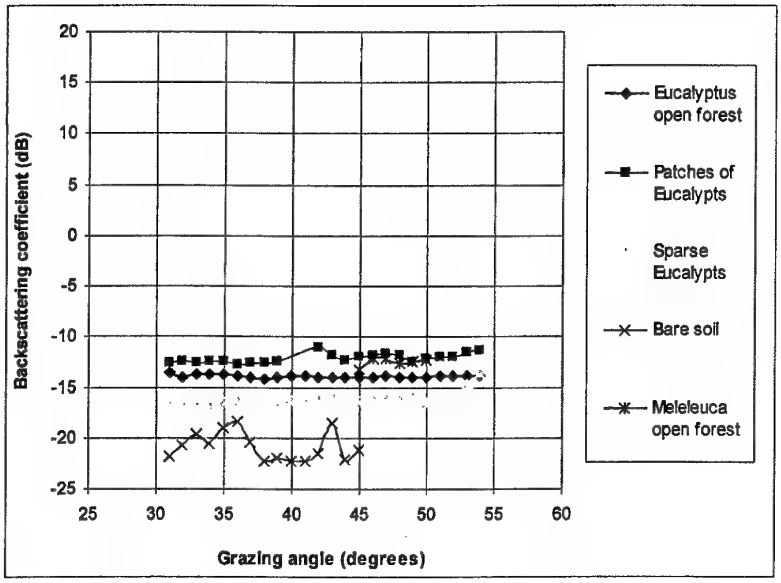

Figure 20: L band VV clutter distribution for each vegetation class as a function of grazing angle (Humpty Doo scene)

The clutter distribution for each vegetation class against the grazing angle is given in Figure 20. Because the variation of the grazing angle is only in the region of 30° to 55°, narrower than the previous two scenes, all types of vegetation show a flat response. The highest clutter returns, from patches of eucalypts (the existence of underwater was possible in November) and melaleuca, are about -12dB whereas the lowest returns of −20dB are from bare soil (including highways/roads). The difference between the two is about 8dB.

4.4 Farewell Site

The Farewell site is also located in Kakadu National Park, at the entrance of the West Alligator River. Dominant species in the scene include mangrove, eucalypts, melaleuca and tussock grassland. The image of the site and its accompanying vegetation classification are shown in Figure 21.

Mangrove communities most commonly occur in areas where the average temperature of the coldest month is higher than 20°C and where the seasonal range does not exceed 10°C. Areas which have a great variety of mangrove species are found along coasts that receive high rainfall, heavy run off and seepage into the intertidal zone from the hinterland. Such areas are commonly subject to extensive sedimentation, which provides a diverse range of substrate types and nutrient levels, which in turn are favorable for mangrove growth. Over 4,000 km^2 of mangroves are found along the 10,953 km NT coastline. This represents around 35% of the 11,600 km^2 of mangroves found throughout Australia (DLPE, 2002). Figure 22 is a photo of tidal flats and

estuarine mangrove, a commonly seen littoral land system in the Top end (Lynch and Wilson 1998).

The clutter distribution for each vegetation class against the grazing angle is plotted in Figure 23. Consistent with previous scenes, the clutter returns from all vegetation classes are flat with respect to grazing angle varying from 29-69°. The dynamic range of vegetation clutter is about 10dB varying from as high as -10dB from the clutter of water front mangrove and wet melaleuca to as low as -20dB from the clutter of bare soil.

The clutter of the river water is interesting to look at and requires a few sentences to interpret. In the Darwin scene, we have seen the clutter signals from open seawater monotonically increase from as low as -22dB at a grazing angle of 20° to as high as 16dB at a grazing angle of 75°. The clutter signals of the river water observed in the Farewell scene however are quite different. As the area is flat, the river water is calm, so the surface of the river water is very smooth. The turbulence of the river water due to tidal variations and wind is therefore several orders smaller than the turbulence of open seawater. As a result, the smooth water surface causes very low clutter signals in the low and plateau grazing angle regions. As seen in Figure 23, the clutter of the river water is typically about 10 to 15dB below the clutter of bare soil, and shows an increasing trend for large grazing angles. It is expected that the clutter of the river water would be much higher than that of seawater if the grazing angle approaches 90°.

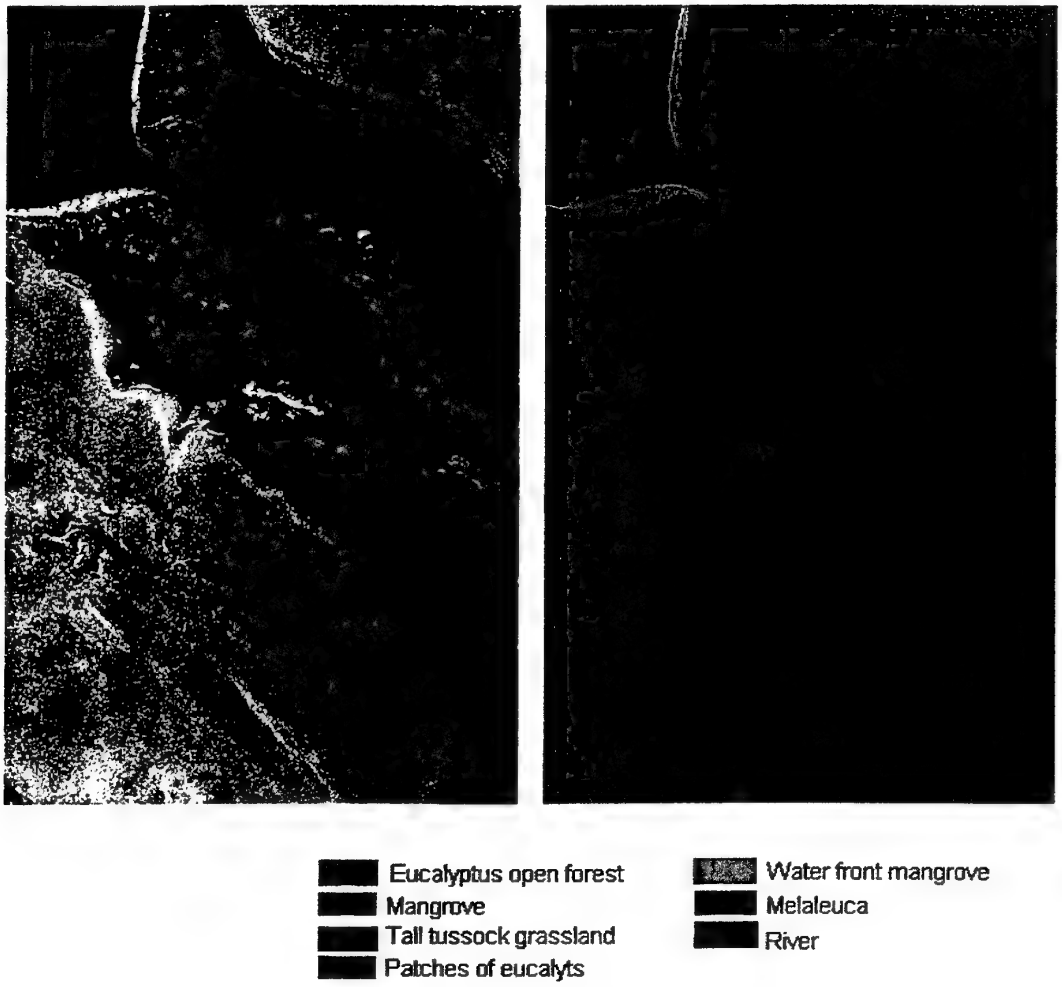

Figure 21: AirSAR L band VV image of the Farewell site and its accompanying vegetation classification. The range direction is from left to right. The image size is 18.4 km by 11.9 km

Figure 22: Tidal flats and estuarine mangrove fringe, commonly seen in the Top End

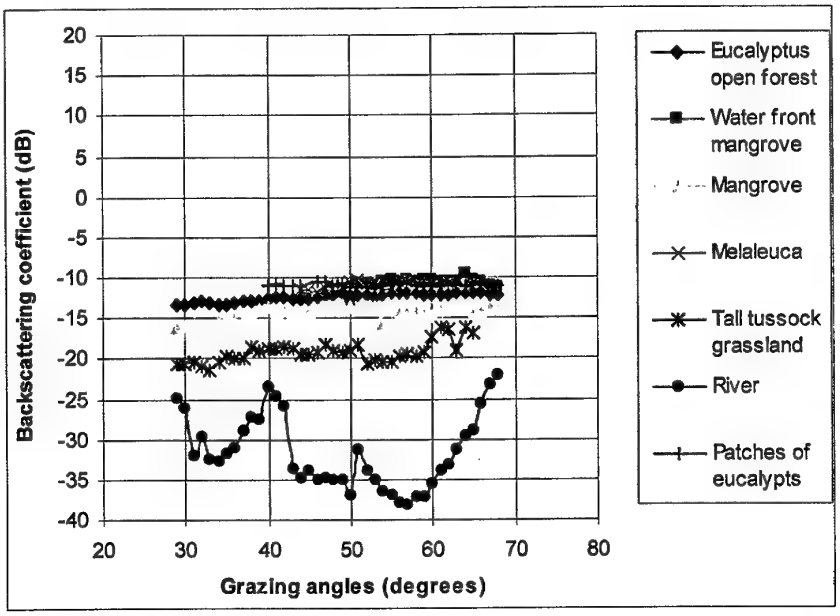

Figure 23: L band VV clutter distribution for each vegetation class as a function of grazing angle (Farewell scene). Because the river water has extra low clutter returns, the value of the vertical axis was extended to –40dB

However, the variation in the river clutter at the grazing angle from 30° to 60° warrants further comment. In the vicinities of 30° and 40° in particular, the observed backscattering coefficient is considerably greater than expected. If the river water is quiet, it is unlikely that there could be stronger Bragg scattering at these angles than at

their neighbouring grazing angles. Figure 24 shows a 3D view of the backscattering coefficient image for the section of the river at the grazing angle of 47° and the section of the river at the grazing angle of 40°, respectively. The distribution of the backscattering coefficient from the river water at the grazing angle of 47° seems uniform whereas the distribution of the backscattering coefficient from the river water at the grazing angle of 40° indicates that there must be some other scattering mechanism(s) in addition to the surface scattering from river water. The exact situation is unknown. However based on our visit to and knowledge of the area, there might be sub-riverbanks created by the tidal movement. The sub-riverbank might be partly above the water with mangrove roots, resulting in higher returns than that from quiet water. The measured clutter values in the vicinity of the grazing angle of 60° is about the same as, whereas the measured values at the grazing angle of 30-40° are a few dB higher than, the values of the calm (State 0)open sea clutter given by Nanthanson, et al, (1999).

On close inspection there was some obvious misclassification in the Farewell scene. At the entrance of the river, an area which should be mangrove has been classified as eucalypts. This was due to lack of difference in the SAR data, so the boundary between the two could not be allocated. This is commonly referred to as the ambiguity in SAR image classification. If the radar cannot differentiate vegetations in terms of the backscattering coefficient, the image processing will also treat them as the same class unless other means are provided.

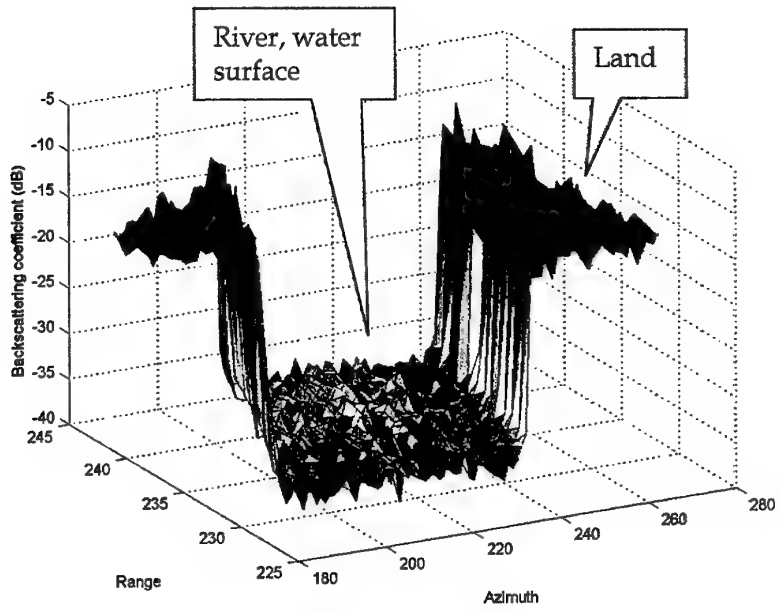

(a)

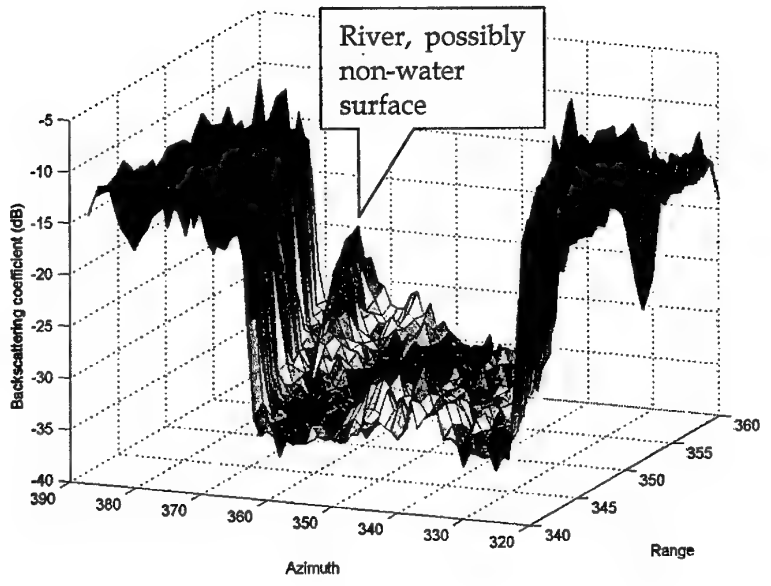

(b)

Figure 24: Backscattering coefficient plotted in 3D for the view of two sections of the river water at the grazing angle of (a) 47° and (b) 40°, respectively

4.5 Combined Data from Four Sites

The backscattering coefficient of the same vegetation class in different scenes is generally consistent. Figure 25 shows the backscattering coefficient of eucalypt open forest/woodland measured in the four scenes. The variation, which is within 2-3dB, apart from scene to scene calibration, is believed to be mainly due to the ground truth conditions. Although all are labelled as eucalypt open forest/woodland, the backscattering coefficient from the Humpty Doo site is 2-3dB lower than that from the other sites. This might be due to the fact that the location of the site is inland, receiving less annual rainfall than other sites, thus trees may tend to be shorter and sparser. In order to have an integrated picture of land clutter, we have combined L band VV clutter distributions from four AirSAR scenes for every type of land cover, and shown the results in Figure 26 and Figure 27, respectively. Figure 26 compares clutter of seawater, open eucalypts, shrub, grassland, bare soil and river water, while Figure 27 shows subtle differences of clutter among various classes of vegetation. In the plateau region, the clutter of vegetated areas shows little dependence on grazing angle. Also in the plateau region, the clutter does show some degree of correlation with the above ground biomass of vegetation. The higher the biomass is, the higher the clutter value. The difference in clutter from eucalyptus open forest/woodland to bare soil is about 8dB. The clutter of calm river water is further 10-15dB lower compared to the clutter of bare soil. For the same species, if there is free surface water (e.g., the area is flooded), the clutter will be a few dB (4-5dB) higher than the clutter without free surface water. One exception is that the clutter of samphire shrub is about the same as the clutter of eucalypts as shown in Figure 26. One possible explanation is that the shrub areas might be flooded which makes higher values of clutter.

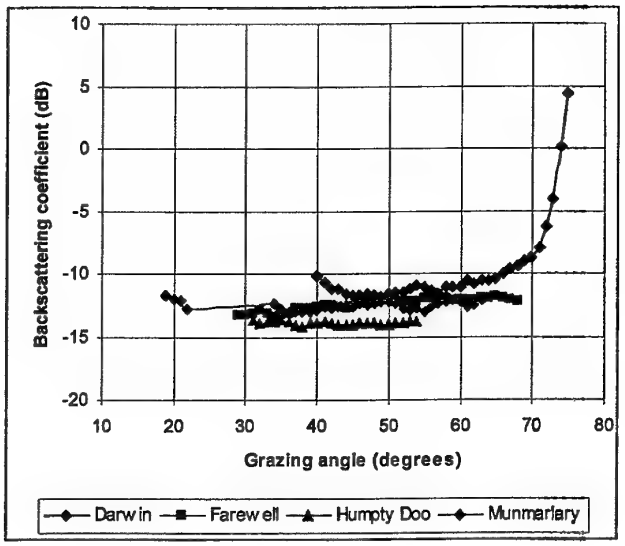

Figure 25: L band VV clutter of eucalypts open forest/woodland measured in four AirSAR scenes

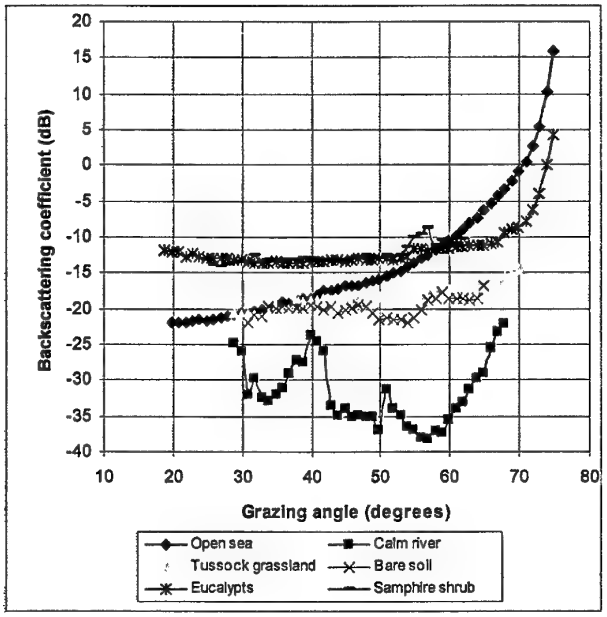

Figure 26: L-band VV clutter distributions for landcover of sea water, woodland, shrub, grassland, bare soil and river water, respectively, combined from four AirSAR scenes

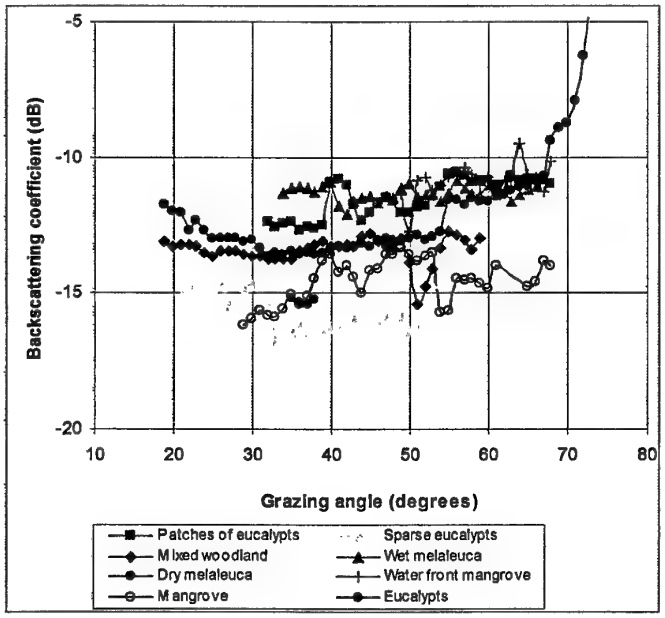

Figure 27: L band VV clutter distributions for different tree communities combined from four AirSAR scenes

5. Summary

Land clutter data at the L band VV polarisation has been studied. The study has not intended to build a land clutter model at this stage, but instead has focused on the understanding and interpretation of various phenomena of clutter in the natural environment and on the indication that the land clutter is different from the sea clutter.

Four AirSAR scenes acquired from the Top End region of Australia have been used for analysis. With an area of more than 60 km^2, these four scenes together have most commonly vegetation communities in the region including eucalyptus open forest/woodland, mixed woodland, melaleuca, mangrove, tussock grassland, bare soil, open seawater and river water. Of these four scenes, two were acquired in the dry season and the other two in the wet season.

A land clutter model without land information may be too general to be used. Realising that clutter depends on not only radar parameters, but also geo-physical parameters, we have used the following steps to carry out the data analysis:

1. Decoding AirSAR data to obtain the VV backscattering coefficient in the ground range;
2. Using SAR segmentation processing techniques to partition an image into uniform polygons;
3. Assigning each polygon a vegetation label with the reference to the vegetation map;
4. Calculating the clutter distribution for each vegetation class against the grazing angle to disclose the characteristics of clutter for the specific vegetation.

The clutter distribution for a specific vegetation class at a specific grazing angle, which depends on both the radar and geo-physical parameters, is another topic. In this report we have only concentrated on the mean value of the clutter.

The analysis has resulted in the following findings:

- Clutter from the open sea monotonically increased with an increase in the grazing angle except when the grazing angle approaches 0°. In the Darwin scene, the sea clutter was as low as -22dB at the grazing angle of 20°, whereas the clutter increased to as high as 16dB at the grazing angle of 75°. The actual values of clutter depend on the wind velocity. According to the recorded wind velocity and in comparison with values of the normalised mean sea clutter given by Nathanson, et al, (1999), the measured values were about 10dB higher. This might be due to significant wave building in the littoral (shallow water effect). This needs a further confirmation in the future.

- Clutter from all vegetation classes exhibited little dependence on the grazing angle in the region of 20-65°. The clutter of a specific vegetation class statistically remained approximately constant in this region. It is worth noting that 20° is not the lowest angle of the plateau region, rather it is the lowest angle where AirSAR data are available. The lowest angle of the plateau region is believed to be about 5 to 10° at L band.

- Clutter was correlated to vegetation biomass, with a high value of about −10dB for eucalyptus and melaleuca open forests and a low value of about −20dB for bare soil. The dynamic range due to the vegetation was about 8-10dB.

- Quiet river water had the lowest clutter at grazing angles of 30° to 65°. The clutter ranged from -35 to -25dB, some 10-15dB below the clutter of bare soil. The measured values at the vicinity of the grazing angle of 60° agree with, whereas the values at the grazing angle of 30-40° are a few dB higher than, the values given by Nathanson, et, al (1999) for the calm (State 0) open sea clutter.

- When the grazing angle increased beyond 70°, all vegetation classes in the Top End demonstrated a rapid increase in clutter signals similar to the pattern of the sea clutter. Because all forests in these scenes had less than 30% canopy closure, surface scattering could still contribute to the clutter. The value of the clutter, compared to the value of the sea clutter, would be expected to be lower, due to attenuation by the canopy layer and understorey vegetation, as well as the lower dielectric constant of the ground surface. At a grazing angle of near 90°, the clutter of the calm river water, if its condition matches sea (e.g., its size is greater than the radar's resolution) would be as higher as +10 to +26dB measured from the calm open seawater at vertical incidence (Nathanson, et, al, 1999).

- These four scenes have not demonstrated a significant difference in the clutter from forests between dry and wet seasons. But we have definitely seen that the return from melaleuca/mangrove with underwater was a few dB (4-5dB) higher than the return from melaleuca/mangrove without underwater.

6. Future Work

The grazing angle of the available AirSAR data ranges only from about 20 to 75°, leaving both ends of a complete curve of reflectivity with respect to grazing angle of 0 to 90° to be fulfilled using other data in the future.

Spatial distribution of land clutter may also be analysed using single-look SAR data. Since SAR synthesises conditions of RAR (real aperture radar), distributions of SAR and RAR data should probably be the same if all parameters (i.e., frequency, polarisation, incidence angle, resolution and signal-to-noise ratio) are the same.

Currently the available AirSAR data were processed as multi-look data, which have compressed the spread of the data distribution. A request for single-look data has been registered with JPL.

Doppler spectrum of the land clutter is low. SAR processing uses the Doppler shift principle to register the received energy to ground pixels to achieve azimuth resolution assuming clutter is static. The Doppler spectrum of clutter is important to the generation of clutter models, so this has to be studied using other available means.

Compared to clutter values for open seawater given in the literature, the AirSAR measured a higher value of seawater in the littoral under the same wind condition. This requires a further confirmation possibly using other source of data.

After all important aspects of land clutter are investigated and studied, a statistical and site-specific land clutter model is to be built.

7. Acknowledgement

We thank Vegetation Mapping Group, Department of Primary Industries, Water and Environment, Australia, and Natural Resources Division, Department of lands, Planning and Environment, Northern Territory, for providing information of land and vegetation for the Northern Territory.

The author thanks Drs A Shaw, J Whitrow and N Stacy for their comments and discussions that have greatly improved the quality and readability of the report.

8. References

1. ANRA (Australian Natural Resources Atlas), *http://audit.ea.gov.au*, 2002.

2. AUSLIG (Australian Surveying and Land Information Group), *Atlas of Australian Resources, Third Series*, Volume 6: *Vegetation*, Canberra, 1990.

3. Billingsley, J B, *Low-Angle Land Clutter Measurements and Empirical Models*, William Andrew Publishing, 2002.

4. Choong, P L, "Modelling airborne L-band radar sea and coastal land clutter," Technical Report, DSTO-TR-0945, the Defence Science Technology Organisation, Australia, 2000.

5. Christensen, N L, E S Kasischke, and M C Dobson, "SAR-derived estimates of above ground biomass in forested landscapes," *Proceedings of IGARSS*, vol. 2, pp. 1209-1212, Maryland, USA, 1990.

6. DIPE (Department of Infrastructure, Planning and Environment), The Northern Territory, *http://www.lpe.nt.gov.au*, 2002.

7. Dobson, M C, F T Ulaby, T Le Toan, A Beaudoin, E S Kasischke, and N Christensen, "Dependence of radar scatter on coniferous forest biomass," *IEEE Trans on Geoscience and Remote Sensing*, vol . 30, no. 2, pp. 412-415, 1992.

8. Dobson, M C, F T Ulaby, L E Pierce, T L Sharik, K M Bergen, J Kellndorfer, J R Kendra, E Li, Y C Lin, A Nashashibi, K Sarabandi, and P Siqueira, "Estimation of forest biophysical characteristics in Northern Michigan with SIR-C/X-SAR," *IEEE Trans on Geoscience and Remote Sensing*, vol . 33, no. 4, pp. 877-894, 1995a.

9. Dobson, M C, L E Pierce, K M Bergen, J Kellndorfer, and F T Ulaby, "Retrieval of above-ground biomass and detection of forest disturbance using SIR-C/X–SAR," *Proceedings of IGARSS*, vol. 2, pp. 987-989, Florence, Italy, 1995b.

10. Dong, Y, "A long wavelength radar backscatter model for forests," PhD thesis, the University of New South Wales, 1995.

11. Dong, Y, B C Forster, and C Ticehurst, "Optimal decomposition of radar polarisation signatures," *IEEE Trans. on Geoscience and Remote Sensing*, vol. 36, no. 3, pp. 933-939, 1998.

12. Dong, Y, B C Forster, and A K Milne, "Segmentation of radar imagery using Gaussian Markov random field model," *International Journal of Remote Sensing*, vol. 20, no. 8, pp. 1617-1639, 1999.

13. Dong, Y, A K Milne, and B C Forster, "Segmentation and classification of vegetated areas using polarimetric SAR image data," *IEEE Trans on Geoscience and Remote Sensing*, vol. 39, no.2, pp. 325-329, Feb 2001.

14. Harrel, P A, L L Bourgeau-Chavez, E S Kasischke, N H F Frence, and N L Christensen, Jr, "Sensitivity of ERS-1 radar data to biomass and standstructure in Alsskan boreal forest", *Remote Sensing of Environment*, vol. 54, pp. 247-260, 1995.

15. Horn, G, A K Milne, and M Finlayson, "Monitoring wetland inundation patterns using Radarsat multitemporal data," *Canadian Journal of Remote Sensing*, vol 26, no 2, pp. 133-137, April 2000.

16. Hsu, C C, R T Shin, J A Kong, A Beaudoin, and T Le Toan, "Application of theoretical model for microwave remote sensing of forest," *Proceedings of IGARSS*, vol. 2, pp. 595-597, Tokyo, Japan, 1993.

17. Imhoff, M L, "Radar backscatter/biomass saturation: Observations and implication for global biomass assessment," *Proceedings of IGARSS*, vol 1, pp. 43-45, Tokyo, Japan, 1993.

18. Karam, M A, F Amar, A K Fung, E Mougin, A Lopes, D M Le Vine, and A Beaudoin, "A microwave polarimetric scattering model for forest canopies based on vector radiative transfer theory," *Remote Sensing of Environment*, vol. 53, pp. 16-30, 1995.

19. Le Toan, T, A Beaudoin, J Riom, and D Guyon, "Relating forest biomass to SAR data," *IEEE Trans on Geoscience and Remote Sensing*, vol. 30. no. 2, pp. 403-411, 1992.

20. Long, M W, *Radar Reflectivity of Land and Sea*, 3rd Edition, Artech House, 2001.

21. Lynch T, and P L Wilson, "Land systems of Arnhem land," Technical Report, No R97/1, Natural Resources Division, Department of Lands, Planning and Environment, Northern Territory, 1998.

22. Morchin, W C, *Airborne Early Warning Radar*, Artech House, 1990.

23. Nathanson, F E, J P Reilly, and M N Cohen, *Radar Design Principles, 2nd Edition*, Scitech Publishing Inc., 1999.

24. Ranson, K J, and G Sun, "Mapping biomass of a northern forest using multifrequency SAR data," *IEEE Trans on Geoscience and Remote Sensing*, vol 32, no 2, pp. 388-396, 1994.

25. Richards, J A, P W Woodgate, and A K Skidmore, "An explanation of enhanced radar backscattering from flooded forests," *International Journal of Remote Sensing*, vol. 8, no. 7, pp. 1093-1100, 1987.

26. Souyris, J C, and T Le Toan, "Inversion of lands forest biomass using SIR-C/X-SAR data," *Proceedings of IGARSS*, vol. 2, pp. 1201-1203, Florence, Italy, 1995.

27. Stogryn, A, "equations for calculating the dielectric constant of saline water," *IEEE Trans Microwave Theory Technology*, vol. MTT-19, pp. 733-736, 1971.

28. Tiangco, P N, "A multi-parameter microwave approach to stand structure and forest biomass estimation," PhD thesis, the University of New South Wales, 1999.

29. Ulaby, F, R Moore, and A Fung, *Microwave Remote Sensing: Active and Passive, Volume II, Radar Remote Sensing and Surface Scattering and Emission Theory*, Artech House, 1982.

Appendix A: Decoding Formulas for JPL AirSAR Compressed Stokes Matrix (CM) Data

Fully polarised SAR data provided by JPL AirSAR group is usually compressed in a special format developed by JPL (JPL, 1995). The commercial image processing software, such as ENVI, provides utilities to decode the compressed data. There is no access to ENVI at EWRD, so both MATLAB and C programs have been written to decode the compressed data.

The 4 by 4 Stokes matrix, with the assumption of reciprocity ($S_{hv} = S_{vh}$), is symmetrical. Expressions for its elements are:

$$M_{11} = \frac{1}{4}\left(S_{hh}^2 + 2S_{hv}^2 + S_{vv}^2\right) \quad \text{(A-1)}$$

$$M_{12} = \frac{1}{4}\left(S_{hh}^2 - S_{vv}^2\right) \quad \text{(A-2)}$$

$$M_{13} = \frac{1}{2}\mathrm{Re}\left\{S_{hh}S_{hv}^* + S_{hv}S_{vv}^*\right\} \quad \text{(A-3)}$$

$$M_{14} = -\frac{1}{2}\mathrm{Im}\left\{S_{hh}S_{hv}^* + S_{hv}S_{vv}^*\right\} \quad \text{(A-4)}$$

$$M_{22} = \frac{1}{4}\left(S_{hh}^2 - 2S_{hv}^2 + S_{vv}^2\right) \quad \text{(A-5)}$$

$$M_{23} = \frac{1}{2}\mathrm{Re}\left\{S_{hh}S_{hv}^* - S_{hv}S_{vv}^*\right\} \quad \text{(A-6)}$$

$$M_{24} = -\frac{1}{2}\mathrm{Im}\left\{S_{hh}S_{hv}^* - S_{hv}S_{vv}^*\right\} \quad \text{(A-7)}$$

$$M_{33} = \frac{1}{2}\mathrm{Re}\left\{S_{hh}S_{vv}^*\right\} + \frac{1}{2}S_{hv}^2 \quad \text{(A-8)}$$

$$M_{34} = -\frac{1}{2}\mathrm{Im}\left\{S_{hh}S_{vv}^*\right\} \quad \text{(A-9)}$$

$$M_{44} = -\frac{1}{2}\mathrm{Re}\left\{S_{hh}S_{vv}^*\right\} + \frac{1}{2}S_{hv}^2 \quad \text{(A-10)}$$

where $\mathrm{Re}\{\cdot\}$ and $\mathrm{Im}\{\cdot\}$ denote real and imaginary parts of a complex value, and * denotes complex conjugate.

The decoding of Stokes matrix elements is given as,

$$M_{11} = \left(\frac{b_2}{254} + 1.5\right) 2^{b_1} \times g \tag{A-11}$$

$$M_{12} = b_3 \frac{M_{11}}{127} \tag{A-12}$$

$$M_{13} = sign(b_4)\left(\frac{b_4}{127}\right)^2 M_{11} \tag{A-13}$$

$$M_{14} = sign(b_5)\left(\frac{b_5}{127}\right)^2 M_{11} \tag{A-14}$$

$$M_{23} = sign(b_6)\left(\frac{b_6}{127}\right)^2 M_{11} \tag{A-15}$$

$$M_{24} = sign(b_7)\left(\frac{b_7}{127}\right)^2 M_{11} \tag{A-16}$$

$$M_{33} = b_8 \frac{M_{11}}{127} \tag{A-17}$$

$$M_{34} = b_9 \frac{M_{11}}{127} \tag{A-18}$$

$$M_{44} = b_{10} \frac{M_{11}}{127} \tag{A-19}$$

$$M_{22} = M_{11} - M_{33} - M_{44} \tag{A-20}$$

where g is a scale factor, which can be find in the header file of the SAR data. Its value is usually equal to 1.

After the Stokes matrix is decoded, the relevant values can be easily found. For example, the VV polarisation backscattering coefficient for the pixel is simply equal to S_{vv}^2 as

$$S_{vv}^2 = M_{11} + M_{22} - 2M_{12} \tag{A-21}$$

Reference:

1. JPL (Jet Propulsion Laboratory), AirSAR integrated processor documentation: Data formats (version 0.01), JPL, Pasadena, 1995.

Appendix B: Grazing Angle, Slant Range and Ground Range

We normally have to consider the curvature of the Earth when determining the ground range of AirSAR data.

As shown in Figure B-1, the radar look angle is θ, height H, slant range L, the Earth's equivalent radius R. Angle ϕ corresponds to the Earth's curvature $\hat{A}\hat{B}$.

$$\frac{R}{\sin\theta} = \frac{L}{\sin\phi} \quad \text{(B-1)}$$

$$\hat{A}\hat{B} = R\phi \quad \text{(B-2)}$$

Let us consider typical AirSAR parameters: $R = 4/3 \times 6378 \times 10^3 m$, $\theta = 71.1^0$ and $L = 26011.99m$ we have

$$\hat{A}\hat{B} = 24609.6m \quad \text{(B-3)}$$

$$\phi = 0.16580739^0 \quad \text{(B-4)}$$

Since $\angle CAB = \phi/2$, we have

$$\overline{AB} = \sin\theta \frac{L}{\sin(90^0 + \phi/2)} = 24609.6m \quad \text{(B-5)}$$

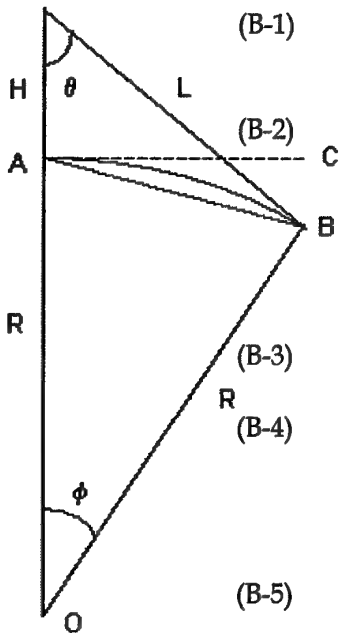

Figure B-1: Ground range determination

To include the effect of the curved propagation paths in calculation the equivalent Earth's radius (4/3 times the real Earth's radius) has been used, so straight lines can then be used to calculate the various true angles and distances (Long, 2001).

Comparing (B-3) and (B-5), we can see that the difference between line $\overline{AB}$ and curvature $\hat{A}\hat{B}$ is minimal. Therefore in the calculation we can use line $\overline{AB}$ for the substitution of $\hat{A}\hat{B}$.

The relationship between ground range G and slant range L (Figure B-2) can be found by

$$\frac{H}{\sin\beta} = \frac{L}{\sin\alpha} = \frac{G}{\sin\theta} \tag{B-6}$$

where β is the grazing angle, $\alpha = 90^0 + \phi/2$.

The header file of JPL AirSAR data provides parameters including height, near incidence angle, near slant range, far incidence angle and far slant range. Sometimes it will be found that these parameters do not exactly match when checking them using the above equations. It might be due to a few digits available in the incidence angle values. If necessary, a small modification might be needed to remove the mismatches. It is suggested that it is preferable to use the slant ranges and height to work out the incident angles by,

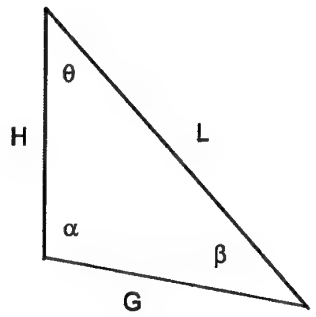

Figure B-2: Ground range and slant range

$$\cos\theta = \frac{L^2 + (H+R)^2 - R^2}{2L(H+R)} \tag{B-7}$$

The grazing angle is

$$\beta = 180^0 - (\theta + 90^0 + \phi/2) \tag{B-8}$$

DISTRIBUTION LIST

L-band VV Clutter Analysis for Natural Land in Northern Territory Areas

Yunhan Dong

AUSTRALIA

		Number of Copies
1. DEFENCE ORGANISATION		
Task Sponsor: OCAEWC-SPO		1
S&T Program		
Chief Defence Scientist	shared copy	1
FAS Science Policy	shared copy	1
AS Science Corporate Management	shared copy	1
Director General Science Policy Development		1
Counsellor Defence Science, London		Doc Data Sheet
Counsellor Defence Science, Washington		Doc Data Sheet
Scientific Adviser to MRDC Thailand		Doc Data Sheet
Scientific Adviser Joint		1
Navy Scientific Adviser		Doc Data Sheet 1 x distribution list
Scientific Adviser Defence Materiel Organisation		Doc Data Sheet 1 x distribution list
Scientific Adviser - Army		Doc Data Sheet 1 x distribution list
Air Force Scientific Adviser		Doc Data Sheet 1 x distribution list
Director Trials		1
Systems Sciences Laboratory		
EWSTIS (soft copy for accession to EWSTIS Web site)		1
Chief, Electronic Warfare and Radar Division		Notification
Research Leader, RF Electronic Warfare		Notification
Research Leader, EW Systems		Notification
Research Leader, EO Electronic Warfare		Notification
Research Leader, Microwave Radar		Notification
Head, ES Systems		Notification
Head, RF Countermeasures		Notification
Head, RF Technologies		Notification

Head, Strategic and Land EW	Notification
Head, Aerospace Systems	Notification
Head, Maritime Systems	Notification
Head, NavWar	Notification
Head, EO Threat Warning	Notification
Head, EO Countermeasures	Notification
Head, EO Systems & Technologies	Notification
Head, Phased Array	Notification
Head, Airborne Radar	Notification
Head, Maritime Radar	Notification
Head, EM Signatures	Notification
Mr Scott Capon, EWRD	1
Yunhan Dong, EWRD,	1
DSTO Library	
Library Edinburgh	1
Australian Archives	1
Capability Systems Division	
Director General Maritime Development	Doc Data Sheet
Director General Aerospace Development	1
Director General Information Capability Development	Doc Data Sheet
Office of the Chief Information Officer	
Chief Information Officer	Doc Data Sheet
Deputy CIO	Doc Data Sheet
Director General Information Policy and Plans	Doc Data Sheet
AS Information Structures and Futures	Doc Data Sheet
AS Information Architecture and Management	Doc Data Sheet
Director General Australian Defence Information Office	Doc Data Sheet
Director General Australian Defence Simulation Office	Doc Data Sheet
Strategy Group	
Director General Military Strategy	Doc Data Sheet
Director General Preparedness	Doc Data Sheet
HQAST	
SO (ASJIC)	Doc Data Sheet
Navy	
SO (SCIENCE), COMAUSNAVSURFGRP, BLD 95,	Doc Data Sheet 1 x distribution list

Garden Island, Locked Bag 12, PYRMONT NSW 2009

Director General Navy Capability,
Performance and Plans, Navy Headquarters — Doc Data Sheet

Director General Navy Strategic Policy and Futures,
Navy Headquarters — Doc Data Sheet

Army

SO (Science), Deployable Joint Force Headquarters
(DJFHQ) (L), MILPO Gallipoli Barracks, Enoggera QLD 4052 — Doc Data Sheet

SO (Science), — Doc Data Sheet + Executive Summary

NPOC QWG Engineer NBCD Combat Development Wing,
Tobruk Barracks, Puckapunyal, 3662 — Doc Data Sheet

Intelligence Program

DGSTA, Defence Intelligence Organisation — 1

Manager, Information Centre DIO — 1

Assistant Secretary Corporate,
Defence Imagery and Geospatial Organisation — Doc Data Sheet

Defence Materiel Organisation

Head Airborne Surveillance and Control — Doc Data Sheet

Head Aerospace Systems Division — Doc Data Sheet

Head Electronic Systems Division — Doc Data Sheet

Head Maritime Systems Division — Doc Data Sheet

Head Land Systems Division — Doc Data Sheet

Australian AEW&C Resident Project Team (Baltimore), — 1
c/- Electronic Sensors and Systems Sector,
Northrop Grumman Corporation.
PO Box 1897 (MS 903),

BALTIMORE MD 21203 USA

Defence Libraries

Library Manager, DLS-Canberra — 1

Manager, DLS - Sydney West — Doc Data Sheet

OUTSIDE AUSTRALIA

INTERNATIONAL DEFENCE INFORMATION CENTRES

US Defense Technical Information Center, — 2

UK Defence Research Information Centre, — 2

Canada Defence Scientific Information Service,	1
NZ Defence Information Centre,	1
ABSTRACTING AND INFORMATION ORGANISATIONS	
Library, Chemical Abstracts Reference Service	1
Engineering Societies Library, US	1
Materials Information, Cambridge Scientific Abstracts, US	1
Documents Librarian, The Center for Research Libraries, US	1
INFORMATION EXCHANGE AGREEMENT PARTNERS	
Acquisitions Unit, Science Reference and Information Service, UK	1
National Aerospace Laboratory, Japan	1
National Aerospace Laboratory, Netherlands	1
SPARES	5

Total number of copies: 33

DEFENCE SCIENCE AND TECHNOLOGY ORGANISATION
DOCUMENT CONTROL DATA

1. PRIVACY MARKING/CAVEAT (OF DOCUMENT)

2. TITLE

L-band VV Clutter Analysis for Natural Land in Northern Territory Areas

3. SECURITY CLASSIFICATION (FOR UNCLASSIFIED REPORTS THAT ARE LIMITED RELEASE USE (L) NEXT TO DOCUMENT CLASSIFICATION)

Document	(U)
Title	(U)
Abstract	(U)

4. AUTHOR(S)

Yunhan Dong

5. CORPORATE AUTHOR

Systems Sciences Laboratory
PO Box 1500
Edinburgh South Australia 5111 Australia

6a. DSTO NUMBER	6b. AR NUMBER	6c. TYPE OF REPORT	7. DOCUMENT DATE
DSTO-RR-0254	AR-012-773	Research Report	May 2003

8. FILE NUMBER	9. TASK NUMBER	10. TASK SPONSOR	11. NO. OF PAGES	12. NO. OF REFERENCES
E-9505-25-95	AIR02/232	OCAEWC-SPO	80	29

13. URL on the World Wide Web

http://www.dsto.defence.gov.au/corporate/reports/ DSTO-RR-0254.pdf

14. RELEASE AUTHORITY

Chief, Electronic Warfare and Radar Division

15. SECONDARY RELEASE STATEMENT OF THIS DOCUMENT

Approved for public release

OVERSEAS ENQUIRIES OUTSIDE STATED LIMITATIONS SHOULD BE REFERRED THROUGH DOCUMENT EXCHANGE, PO BOX 1500, EDINBURGH, SA 5111

16. DELIBERATE ANNOUNCEMENT

No Limitations

17. CITATION IN OTHER DOCUMENTS Yes

18. DEFTEST DESCRIPTORS

Ground clutter
Scattering
Radar images
Synthetic aperture radar
Vegetation

19. ABSTRACT

Land clutter is statistical by nature, and its values vary in many different dimensions. This report analyses land clutter characteristics using AirSAR data for airborne L band VV polarised radars. In particular, the report concentrates on the distribution of clutter values with respect to grazing angles for various vegetation communities typically seen in the Northern Territory region in Australia. Future reports will adress wider aspects, including spatial distributions and Doppler spectrums of clutter sufficient to enable the generation of radar clutter models.